Residual-type a posteriori error estimator for a quasi-static Signorini contact problem

Mirjam Walloth
Fachbereich Mathematik, TU Darmstadt
Dolivostraße 15, 64293 Darmstadt, *walloth@mathematik.tu-darmstadt.de*

Abstract

We present a new residual-type a posteriori estimator for a quasi-static Signorini problem. The theoretical results are derived for two and three-dimensional domains and the case of non-discrete gap functions is addressed. We derive global upper and lower bounds with respect to an error notion which measures the error in the displacements, the velocities and a suitable approximation of the contact forces. Further, local lower bounds for the spatial error in each time step are given. The estimator splits in temporal and spatial contributions which can be used for the adaptation of the time step as well as the mesh size. In the derivation of the estimator the local properties of the solution are exploited such that the spatial estimator has no contributions related to the non-linearities in the interior of the actual time-dependent contact zone but gives rise to an appropriate refinement of the free boundary zone.

Key words. Quasi-static contact problem, Signorini problem, viscoelasticity, residual-type a posteriori error estimator, Galerkin functional, full-contact

1 Introduction

The numerical simulation plays a substantial role in understanding processes and effects in natural sciences and engineering. Quantities that are not readily obtained from measurements because experiments are too expensive, too difficult or even impossible can be approximated numerically. Especially in medicine the numerical simulation is in great demand, whenever the ethical dimension has to be considered. We are interested in the simulation of viscoelastic contact problems. Biological tissue as cartilage, bones and tendons are examples of viscoelastic materials.

In this work we consider a quasi-static contact problem which models the contact between a linear viscoelastic material and a rigid body. The linear viscoelastic material obeys the Kelvin-Voigt model. Viscoelasticity means that the material behavior shows both elastic and viscous features and thus the stress tensor depends on the displacements as well as the velocities. The resulting quasi-static contact problem gives rise to a time-dependent variational inequality.

A posteriori error estimators which are equivalent to the error are in great demand in the numerical simulation to determine regions with less regular or even singular behavior. These information can be used for mesh adaptation. For

the simulation of complex processes adaptive mesh generation is important to improve the quality of the discrete solution for given computational resources.
A popular estimator for linear elliptic problems, which appears attractive in view of its simplicity, is the standard residual estimator [23, 25]. It is explicitly computable from the given data and the discrete finite element solution and constitutes an upper as well as a lower bound of the error at least up to so-called oscillation terms of higher order. Thus, it is equivalent to the error. For the prototype of variational inequalities, the obstacle problem, techniques of standard residual-estimation have been extended in [11, 14, 19, 20, 22] to derive residual-type a posteriori estimators. Further, for the Signorini contact problem residual-type a posteriori estimators have been derived in [12, 16, 27].
For the heat equation as an example of time-dependent problems a residual a posteriori error estimator has been derived in [24], see also [25] for parabolic problems. Therein global in space and time upper bounds and global in space and local in time lower bounds have been proven with respect to the same error measure. The error in the velocities is measured in the H^{-1}-norm and the error in the displacements in the H^1-norm. An a posteriori error analysis for linear viscoelastic problems without constraints can be found in [7]. Therein an upper bound for the H^1-norm of the error in the velocities and in the displacements is derived. The error measure for the global lower bound is different. In each time step a local lower bound is given for the spatial error. In [8] a normal compliance viscoelastic contact problem is considered which means that the non-penetration condition is weakly imposed by a penalty method so that an equality instead of an inequality is considered. Thus, the derivation of the estimator is similar to [7]. In [7,8,24] the estimator splits in a temporal and a spatial contribution. A posteriori error analysis for a time-dependent variational inequality can be found in [18], where a parabolic obstacle problem is considered. In the error measure for the upper bound not only the H^1-norm of the error in the displacements but also a dual norm of the error in the velocity and in the contact force is taken. For the standard estimator contributions a local lower bound for the spatial error in each time step is given.
In this work we derive a residual-type a posteriori error estimator for the time-dependent variational inequality of the linear viscoelastic Signorini contact problem. To the best of our knowledge that is the first residual-type estimator for this kind of contact problem without a regularization of the non-penetration condition. We derive a global in space and time upper bound and a global in space and local in time lower bound with respect to the same error measure. Further we derive local lower bounds for the spatial error in each time step with respect to a slightly different measure. The theory is derived for two- and three-dimensional domains and even non-discrete gap functions are considered. The works [16, 22] on elliptic obstacle and contact problems reveal that sharp a posteriori error estimators for variational inequalities can be derived by involving the error in the constraining forces in the error measure. Thus, we consider an error measure representing the error in the displacements, velocities and constraining forces.
A key ingredient in the derivation of efficient and reliable residual-type a posteriori estimators for obstacle and contact problems [9, 16, 22] is the Galerkin functional which replaces the linear residual of elliptic unconstrained problems. The Galerkin functional as well as the error measure consider the error in the displacements and velocities as well as the difference between the constraining

force $\boldsymbol{\lambda}$ and a suitable discrete approximation $\tilde{\boldsymbol{\lambda}}_{\mathrm{m}}^{\tau}$ which we call quasi-discrete contact force. The definition of this approximation reflecting the local structure of the solution is very crucial for the proof of the lower bound as well as for the localization of the estimator contributions, i.e. to avoid over-refinement. Therefore we distinguish between areas of the contact boundary where the bodies are partially or fully in contact, so-called semi- and full-contact areas. The quasi-discrete contact force as well as the definition of full-contact depend on the evolution in time which is in contrast to [18]. The rate-dependency of full-contact is new and enables to tackle the proof of lower bound.
The temporal as well as spatial estimators reduce to standard estimator contributions if no contact occurs. The estimator contributions addressing the non-linearity are related to the contact stresses and the complementarity condition with respect to the solution in two subsequent time steps. Due to the fact that we exploit the local structure we avoid any spatial estimator contributions related to the non-linearity in the area of full-contact. In consequence, the estimator perceives that at the boundary which is in full-contact, where the solution equals the discrete gap function, adaptive mesh refinement cannot improve the solution. In the case of arbitrary non-discrete gap functions estimator contributions related to the obstacle approximation and constraint violation occur.
Finally, numerical examples confirm our theoretical results. We present the convergence rate of the estimator compared to uniform refinement. Further, the adaptively refined meshes in each time step and the adaptation of the time step size are shown.

2 The Signorini contact problem with linear viscoelastic material

We consider the contact of a linear viscoelastic body with a rigid obstacle. Linear viscoelastic materials are time-dependent. The variable in time is denoted by t and the time interval of interest is $I = [0, T]$. The linear viscoelastic body is represented by a Lipschitz domain $\Omega \subset \mathbb{R}^d$ where $d = 2, 3$ is the dimension. The whole boundary Γ is subdivided into three disjoint parts, the Neumann boundary Γ_N which is an open subset of Γ, the potential contact boundary Γ_C and the Dirichlet boundary Γ_D which are both closed subsets of Γ. Each material particle in the closure $\bar{\Omega}$ is identified with a point $\boldsymbol{x} = (x_1, \ldots, x_d)^T$. Throughout this work we denote all quantities which refer to tensors of order ≥ 1 by bold symbols as, e.g., the displacements $\boldsymbol{u}$ which are vector-valued. Their components are printed in normal type and are indicated by subindices, e.g., u_i. The summation convention is enforced and $\boldsymbol{e}_i$, $i = 1, \ldots, d$, denote the Cartesian basis vectors of $\mathbb{R}^d$ such that, e.g., $\boldsymbol{u} = u_i \boldsymbol{e}_i$. The derivative in time is denoted with a dot above, i.e. the velocities are denoted by $\dot{\boldsymbol{u}}$.
The deformable body consists of linear viscoelastic material obeying the Kelvin-Voigt model, see e.g. [13, Chapter 6.3], [5, Chapter 5.1]. The linearized strain tensor is given by

$$\boldsymbol{\epsilon}(\boldsymbol{u}) = \frac{1}{2}\left(\nabla \boldsymbol{u} + (\nabla \boldsymbol{u})^T\right).$$

For the linear stress-strain relation we need the fourth order viscosity tensor $\boldsymbol{\mathcal{A}} = (a_{ijkl})$ and the fourth order elasticity tensor $\boldsymbol{\mathcal{B}} = (b_{ijkl})$. They are both

linear, bounded, symmetric and positively definite.
The stress tensor $\boldsymbol{\sigma}$ obeys the following constitutive law

$$\boldsymbol{\sigma} := \boldsymbol{\mathcal{A}}\boldsymbol{\epsilon}(\dot{\boldsymbol{u}}) + \boldsymbol{\mathcal{B}}\boldsymbol{\epsilon}(\boldsymbol{u}).$$

Let λ and μ be the Lamé constants of linear elasticity, then $\boldsymbol{\mathcal{B}}\boldsymbol{\epsilon} = \lambda \mathrm{tr}(\boldsymbol{\epsilon})\boldsymbol{id} + 2\mu\boldsymbol{\epsilon}$. Further, let η be the shear viscosity, ζ the bulk viscosity, then $\boldsymbol{\mathcal{A}}\boldsymbol{\epsilon} = \lambda_V \mathrm{tr}(\boldsymbol{\epsilon})\boldsymbol{id} + 2\eta\boldsymbol{\epsilon}$ with $\lambda_V := (\zeta - \frac{2}{3}\eta)$.
When two solid bodies come into contact they do not penetrate each other. If the displacements are small like in linear viscoelasticity the non-penetration condition can be approximated by the so-called linearized non-penetration condition, see e.g. [6] and [15]. The gap function describing the distance between the viscoelastic body and the rigid body is given by $g : \Gamma_C \times I \to \mathbb{R}$ and the direction of constraints is denoted by $\boldsymbol{\nu}$. Thus, the linearized non-penetration condition is $u_\nu \leq g$ where $u_\nu := \boldsymbol{u} \cdot \boldsymbol{\nu}$. The non-penetration condition evokes so-called contact stresses which are boundary stresses in direction of the constraints at the actual contact boundary. We use the notation $\hat{\boldsymbol{\sigma}}(\boldsymbol{u}) := \boldsymbol{\sigma}(\boldsymbol{u})\boldsymbol{n}$ for boundary stresses where $\boldsymbol{n}$ is the unit outward normal to the boundary. Hence, the contact stresses are given by $\hat{\sigma}_\nu(\boldsymbol{u}) := \hat{\boldsymbol{\sigma}}(\boldsymbol{u}) \cdot \boldsymbol{\nu}$. As we neglect frictional effects the frictional stresses $\hat{\boldsymbol{\sigma}}_{\tan}(\boldsymbol{u}) := \hat{\boldsymbol{\sigma}}(\boldsymbol{u}) - \hat{\sigma}_\nu(\boldsymbol{u}) \cdot \boldsymbol{\nu}$ are assumed to be zero.
The linear viscoelastic body might be subjected to a volume force density $\boldsymbol{f}$, to surface forces $\boldsymbol{\pi}$ and to Dirichlet values $\boldsymbol{u}_D$. The complete problem formulation is given in Problem 1.

Problem 1. *Strong formulation of the viscoelastic Signorini contact problem Find a displacement field $\boldsymbol{u} : \Omega \times \bar{I} \to \mathbb{R}^d$ such that*

$$\begin{array}{rcll}
-\mathrm{div}\boldsymbol{\sigma}(\boldsymbol{u}) & = & \boldsymbol{f} & \textit{in} \quad \Omega \times I \\
\hat{\boldsymbol{\sigma}}(\boldsymbol{u}) & = & \boldsymbol{\pi} & \textit{on} \quad \Gamma_N \times I \\
\boldsymbol{u} & = & \boldsymbol{u}_D & \textit{on} \quad \Gamma_D \times I \\
u_\nu & \leq & g & \textit{on} \quad \Gamma_C \times I \\
\hat{\sigma}_\nu & \leq & 0 & \textit{on} \quad \Gamma_C \times I \\
(u_\nu - g) \cdot \hat{\sigma}_\nu(\boldsymbol{u}) & = & 0 & \textit{on} \quad \Gamma_C \times I \\
\hat{\boldsymbol{\sigma}}_{\tan}(\boldsymbol{u}) & = & \boldsymbol{0} & \textit{on} \quad \Gamma_C \times I \\
\boldsymbol{u}(0) & = & \boldsymbol{u}^0 & \textit{in} \quad \Omega
\end{array}$$

2.1 Weak formulation

In order to obtain the weak formulation in space we define for each time t the weak solution space $\boldsymbol{\mathcal{H}} := \{\boldsymbol{v} \in \boldsymbol{H}^1(\Omega) \mid \mathrm{tr}|_{\Gamma_D}(\boldsymbol{v}) = \boldsymbol{u}_D(t) \text{ a.e. on } \Gamma_D\}$ which is a subset of $\boldsymbol{H}^1(\Omega) := (H^1(\Omega))^d$ where tr is the trace operator. For convenience in the discrete approximation of the Dirichlet values we assume $\boldsymbol{u}_D$ to be continuous and piecewise linear in space as well as in time. The space of test functions is given by $\boldsymbol{\mathcal{H}}_0 := \{\boldsymbol{\varphi} \in \boldsymbol{H}^1(\Omega) \mid \mathrm{tr}|_{\Gamma_D}(\boldsymbol{\varphi}) = \boldsymbol{0} \text{ a.e. on } \Gamma_D\}$. Whenever it is clear from the context that the restriction to the boundary requires the trace operator we omit the special notation. Under the assumption $g(t) \in H^{\frac{1}{2}}(\Gamma_C)$ for each $t \in I$ we can define the admissible set $\boldsymbol{\mathcal{K}}(t) := \{\boldsymbol{v} \in \boldsymbol{\mathcal{H}} \mid v_\nu \leq g(t) \text{ a.e. on } \Gamma_C\}$. The directions of constraints $\boldsymbol{\nu}$ are assumed to be constant in space and time and are given by a measurable vector field with absolute value $|\boldsymbol{\nu}(\boldsymbol{x})| = 1$. The L^2-norm and its scalar product are denoted by $\|\cdot\|$ and $\langle\cdot,\cdot\rangle$ without any subindex. The duality pairing between H^1 and its dual H^{-1} is given by $\langle\cdot,\cdot\rangle_{-1,1}$ and the corresponding norms are $\|\cdot\|_1$ and $\|\cdot\|_{-1}$. The duality pairing between $H^{\frac{1}{2}}$ and its dual $H^{-\frac{1}{2}}$ is denoted with $\langle\cdot,\cdot\rangle_{-\frac{1}{2},\frac{1}{2}}$ and the corresponding norms are $\|\cdot\|_{\frac{1}{2}}$ and $\|\cdot\|_{-\frac{1}{2}}$. Later on, we need restrictions to subdomains which are indicated by a further subindex, e.g., $\|\cdot\|_{1,\omega}$ for $\omega \subset \Omega$. We assume the force density $\boldsymbol{f}(t)$ and the Neumann data $\boldsymbol{\pi}(t)$ to be L^2- functions on Ω or Γ_N, respectively. We abbreviate $\left\langle \tilde{\boldsymbol{f}}, \boldsymbol{\varphi} \right\rangle_{-1,1} := \langle \boldsymbol{f}, \boldsymbol{\varphi}\rangle + \langle \boldsymbol{\pi}, \boldsymbol{\varphi}\rangle_{\Gamma_N}$.

Problem 2 (Variational inequality)**.** *Find $\boldsymbol{u} : \bar{I} \to \boldsymbol{\mathcal{H}}$ with $\boldsymbol{u}(0) = \boldsymbol{u}^0$ such that for a.e. $t \in I$, $\boldsymbol{u}(t) \in \boldsymbol{\mathcal{K}}(t)$ fulfills*

$$\begin{aligned}\langle \boldsymbol{\mathcal{A}}\boldsymbol{\epsilon}(\dot{\boldsymbol{u}}(t)), \boldsymbol{\epsilon}(\boldsymbol{v}) - \boldsymbol{\epsilon}(\boldsymbol{u}(t))\rangle + \langle \boldsymbol{\mathcal{B}}\boldsymbol{\epsilon}(\boldsymbol{u}(t)), \boldsymbol{\epsilon}(\boldsymbol{v}) - \boldsymbol{\epsilon}(\boldsymbol{u}(t))\rangle \\ \geq \left\langle \tilde{\boldsymbol{f}}(t), \boldsymbol{v} - \boldsymbol{u}(t) \right\rangle_{-1,1}, \quad \forall \boldsymbol{v} \in \boldsymbol{\mathcal{K}}(t).\end{aligned}$$

We define the contact force density in the continuous setting by

$$\langle \boldsymbol{\lambda}(t), \boldsymbol{\varphi}\rangle_{-1,1} := \langle \boldsymbol{f}(t), \boldsymbol{\varphi}\rangle + \langle \boldsymbol{\pi}(t), \boldsymbol{\varphi}\rangle_{\Gamma_N} - \langle \boldsymbol{\mathcal{A}}\boldsymbol{\epsilon}(\dot{\boldsymbol{u}}(t)), \boldsymbol{\epsilon}(\boldsymbol{\varphi})\rangle - \langle \boldsymbol{\mathcal{B}}\boldsymbol{\epsilon}(\boldsymbol{u}(t)), \boldsymbol{\epsilon}(\boldsymbol{\varphi})\rangle .$$

From an optimization point of view $\boldsymbol{\lambda}$ is the Lagrange multiplier while from a physical point of view $\boldsymbol{\lambda}$ has the meaning of a constraining force density on Γ_C. The contact force density is directly related to the contact stresses

$$\langle \boldsymbol{\lambda}(t), \boldsymbol{\varphi}\rangle_{-1,1} = -\langle \hat{\sigma}_\nu(\boldsymbol{u}(t)), \varphi_\nu\rangle_{-\frac{1}{2},\frac{1}{2}}$$

which follows from the generalized Green's formula. Due to the variational inequality the contact force density fulfills the weak sign condition

$$\langle \boldsymbol{\lambda}, \boldsymbol{v} - \boldsymbol{u}(t)\rangle_{-1,1} \leq 0.$$

For $k \in \mathbb{N}$, $1 \leq p \leq \infty$ we denote the Bochner spaces by

$$\boldsymbol{W}^{k,p}(I;\boldsymbol{\mathcal{H}}) := \{\boldsymbol{v} \in \boldsymbol{L}^p(I;\boldsymbol{\mathcal{H}}) \mid \|v^{(j)}\|_{L^p(I,\mathcal{H})} < \infty,\ \forall j \leq k\}$$

with

$$\|\boldsymbol{v}\|_{W^{k,p}(I;\mathcal{H})} := \left(\int_I \sum_{0 \leq j \leq k} \|v^{(j)}(t)\|^p_{\mathcal{H}}\, dt\right)^{\frac{1}{p}}$$

or

$$\|\boldsymbol{v}\|_{W^{k,\infty}(I,\mathcal{H})} := \max_{0\leq j\leq k} \operatorname{ess\,sup}_{t\in I}\|v^{(j)}\|_{\mathcal{H}}.$$

In this work we assume $\boldsymbol{f} \in W^{1,1}(I, \boldsymbol{L}^2)$, $\boldsymbol{\pi} \in W^{1,1}(I, \boldsymbol{L}^2(\Gamma_N))$ and $g \in W^{1,\infty}(I, H^{\frac{1}{2}}(\Gamma_C))$. An existence and uniqueness result can be found in [13, Theorem 9.3] under the assumption that $\boldsymbol{f} \in W^{1,1}(I, \boldsymbol{L}^2)$, $\boldsymbol{\pi} \in W^{1,1}(I, \boldsymbol{L}^2(\Gamma_N))$, $\boldsymbol{u}_D = g = 0$. The regularity of the solution is $\boldsymbol{u} \in W^{1,\infty}(I;\boldsymbol{\mathcal{H}})$ and thus $\boldsymbol{\lambda} \in L^\infty(I;\boldsymbol{H}^{-1})$. For some cases of time-dependent convex sets $\boldsymbol{\mathcal{K}}(t)$, especially $g \neq 0$, an existence and uniqueness result can be found in [4, Chapter4.3].

2.2 Spatially semi-discrete formulation

In the spatially discrete setting we assume the domain Ω to be polygonal and the grid is a regular simplicial mesh $\mathfrak{M}$, taken from a shape-regular family. The polygonal boundary segments $\Gamma_D, \Gamma_C, \Gamma_N$ are resolved by the mesh, meaning that their boundaries $\partial\Gamma_C, \partial\Gamma_N, \partial\Gamma_D$ are either nodes $\boldsymbol{p}$ or edges. The set of nodes $\boldsymbol{p}$ is given by $\mathfrak{N}_\mathfrak{m}$ and we distinguish between the set $\mathfrak{N}_\mathfrak{m}^D$ of nodes on the Dirichlet boundary, the set $\mathfrak{N}_\mathfrak{m}^N$ of nodes at the Neumann boundary, the set $\mathfrak{N}_\mathfrak{m}^C$ of nodes at the potential contact boundary and the set of interior nodes $\mathfrak{N}_\mathfrak{m}^I$.
For the approximation of $\boldsymbol{\mathcal{H}}$, we use linear finite elements. The space of linear finite elements which are zero on the Dirichlet boundary is denoted with

$$\boldsymbol{\mathcal{H}}_{\mathfrak{m},0} := \{\boldsymbol{\varphi}_\mathfrak{m} \in \boldsymbol{\mathcal{C}}^0(\bar{\Omega}) \mid \forall \mathfrak{e} \in \mathfrak{M},\ \boldsymbol{\varphi}_\mathfrak{m}|_\mathfrak{e} \in \boldsymbol{P}_1(\mathfrak{e}) \text{ and } \boldsymbol{\varphi}_\mathfrak{m} = \boldsymbol{0} \text{ on } \Gamma_D\}$$

and the space with incorporated Dirichlet values $\boldsymbol{u}_D$ is

$$\boldsymbol{\mathcal{H}}_\mathfrak{m} := \{\boldsymbol{v}_\mathfrak{m} \in \boldsymbol{\mathcal{C}}^0(\bar{\Omega}) \mid \forall \mathfrak{e} \in \mathfrak{M},\ \boldsymbol{v}_\mathfrak{m}|_\mathfrak{e} \in \boldsymbol{P}_1(\mathfrak{e}) \text{ and } \boldsymbol{v}_\mathfrak{m} = \boldsymbol{u}_D \text{ on } \Gamma_D\}.$$

The nodal basis functions of the finite element spaces are denoted by ϕ_p. Hence, a discrete vector quantity has the representation

$$\boldsymbol{\varphi}_\mathfrak{m} = \sum_{p \in \mathfrak{N}_\mathfrak{m}} \sum_{i=1}^{d} \varphi_{\mathfrak{m},i}(\boldsymbol{p})\phi_p \boldsymbol{e}_i.$$

As the direction of constraints $\boldsymbol{\nu}$ is constant, $v_{\mathfrak{m},\nu} = \boldsymbol{v}_\mathfrak{m} \cdot \boldsymbol{\nu}$ is a linear finite element function on Γ_C. Let $g_\mathfrak{m}(t)$ be a discrete approximation of the gap function $g(t)$ and $\boldsymbol{\mathcal{K}}_\mathfrak{m}(t)$ the discrete admissible set given by

$$\boldsymbol{\mathcal{K}}_\mathfrak{m}(t) := \{\boldsymbol{v}_\mathfrak{m} \in \boldsymbol{\mathcal{H}}_\mathfrak{m} \mid v_{\mathfrak{m},\nu} \leq g_\mathfrak{m}(t) \text{ on } \Gamma_C\}.$$

We note that $\boldsymbol{\mathcal{K}}_\mathfrak{m} \subset \boldsymbol{\mathcal{K}}$ if $g = g_\mathfrak{m}$.
The spatially semi-discrete scheme of Problem 2 is given by

Problem 3 (Spatially discrete variational inequality)**.** *Find* $\boldsymbol{u}_\mathfrak{m} : \bar{I} \to \boldsymbol{\mathcal{H}}_\mathfrak{m}$ *with* $\boldsymbol{u}_\mathfrak{m}(0) = \boldsymbol{u}_\mathfrak{m}^0$ *such that for a.e.* $t \in I$*,* $\boldsymbol{u}_\mathfrak{m}(t) \in \boldsymbol{\mathcal{K}}_\mathfrak{m}(t)$ *fulfills*

$$\begin{aligned} &\langle \boldsymbol{\mathcal{A}}\boldsymbol{\epsilon}\left(\dot{\boldsymbol{u}}_\mathfrak{m}(t)\right), \boldsymbol{\epsilon}\left(\boldsymbol{v}_\mathfrak{m}\right) - \boldsymbol{\epsilon}\left(\boldsymbol{u}_\mathfrak{m}(t)\right)\rangle + \langle \boldsymbol{\mathcal{B}}\boldsymbol{\epsilon}\left(\boldsymbol{u}_\mathfrak{m}(t)\right), \boldsymbol{\epsilon}\left(\boldsymbol{v}_\mathfrak{m}\right) - \boldsymbol{\epsilon}\left(\boldsymbol{u}_\mathfrak{m}(t)\right)\rangle \\ &\qquad \geq \left\langle \tilde{\boldsymbol{f}}(t), \boldsymbol{v}_\mathfrak{m} - \boldsymbol{u}_\mathfrak{m}(t) \right\rangle_{-1,1} \qquad \forall \boldsymbol{v}_\mathfrak{m} \in \boldsymbol{\mathcal{K}}_\mathfrak{m}(t). \end{aligned}$$

Similar to the continuous case we refer to [13, Chapter 9.3] for an existence and uniqueness result and also for a convergence result.

2.3 Fully-discrete formulation

To discretize in time we use the implicit Euler scheme. At each discrete time t^n the solution is denoted by $\boldsymbol{u}_\mathfrak{m}^n$, the forces by $\boldsymbol{f}^n = \boldsymbol{f}(t^n)$, $\boldsymbol{\pi}^n = \boldsymbol{\pi}(t^n)$ and the gap function by $g_\mathfrak{m}^n = g_\mathfrak{m}(t^n)$. The admissible set is given by $\boldsymbol{\mathcal{K}}_\mathfrak{m}^n = \boldsymbol{\mathcal{K}}_\mathfrak{m}(t^n)$. For each time interval $(t^{n-1}, t^n]$ we define the time step size $\tau^n := t^n - t^{n-1}$ and the linearly interpolated solution $\boldsymbol{u}_\mathfrak{m}^\tau := \frac{t^n - t}{\tau^n}\boldsymbol{u}_\mathfrak{m}^{n-1} + \left(1 - \frac{t^n - t}{\tau^n}\right)\boldsymbol{u}_\mathfrak{m}^n$ and it's derivative $\dot{\boldsymbol{u}}_\mathfrak{m}^\tau := \delta\boldsymbol{u}_\mathfrak{m}^n := \frac{\boldsymbol{u}_\mathfrak{m}^n - \boldsymbol{u}_\mathfrak{m}^{n-1}}{\tau^n}$. Further, we define the linearly interpolated gap function $g_\mathfrak{m}^\tau := \frac{t^n - t}{\tau^n} g_\mathfrak{m}^{n-1} + \left(1 - \frac{t^n - t}{\tau^n}\right) g_\mathfrak{m}^n$ and the piecewise constant in time approximations $\boldsymbol{f}^\tau := \boldsymbol{f}^n$, $\boldsymbol{\pi}^\tau := \boldsymbol{\pi}^n$ on $(t^{n-1}, t^n]$. We define $\left\langle \tilde{\boldsymbol{f}}^n, \boldsymbol{\varphi} \right\rangle_{-1,1} := \langle \boldsymbol{f}^n, \boldsymbol{\varphi}\rangle + \langle \boldsymbol{\pi}^n, \boldsymbol{\varphi}\rangle_{\Gamma_N}$ and $\tilde{\boldsymbol{f}}^\tau$, respectively.

Problem 4 (Fully-discrete variational inequality)**.** *For each $n = 1, \ldots, N$ find $\boldsymbol{u}_{\mathfrak{m}}^n \in \boldsymbol{\mathcal{K}}_{\mathfrak{m}}^n$ fulfilling*

$$\begin{aligned}\left\langle \boldsymbol{\mathcal{A}}\boldsymbol{\epsilon}\left(\delta \boldsymbol{u}_{\mathfrak{m}}^n\right), \boldsymbol{\epsilon}\left(\boldsymbol{v}_{\mathfrak{m}}\right) - \boldsymbol{\epsilon}\left(\boldsymbol{u}_{\mathfrak{m}}^n\right)\right\rangle + \left\langle \boldsymbol{\mathcal{B}}\boldsymbol{\epsilon}\left(\boldsymbol{u}_{\mathfrak{m}}^n\right), \boldsymbol{\epsilon}\left(\boldsymbol{v}_{\mathfrak{m}}\right) - \boldsymbol{\epsilon}\left(\boldsymbol{u}_{\mathfrak{m}}^n\right)\right\rangle \\ \geq \left\langle \tilde{\boldsymbol{f}}^n, \boldsymbol{v}_{\mathfrak{m}} - \boldsymbol{u}_{\mathfrak{m}}^n \right\rangle_{-1,1}, \quad \forall \boldsymbol{v}_{\mathfrak{m}} \in \boldsymbol{\mathcal{K}}_{\mathfrak{m}}^n\end{aligned}$$

with $\boldsymbol{u}_{\mathfrak{m}}^\tau(0) = \boldsymbol{u}_{\mathfrak{m}}^0$.

The unique solvability of the fully-discrete variational inequality of Problem 4 in each time step follows from the Theorem of Lions and Stampacchia [17]. But following [13] there exist up to now no a priori error estimates for the fully discrete solution.
In each time step the discrete contact force density is given by

$$\langle \boldsymbol{\lambda}_{\mathfrak{m}}^n, \boldsymbol{\varphi}_{\mathfrak{m}}\rangle_{-1,1} := \langle \boldsymbol{f}^n, \boldsymbol{\varphi}_{\mathfrak{m}}\rangle + \langle \boldsymbol{\pi}^n, \boldsymbol{\varphi}_{\mathfrak{m}}\rangle_{\Gamma_N} - \langle \boldsymbol{\mathcal{A}}\boldsymbol{\epsilon}(\delta \boldsymbol{u}_{\mathfrak{m}}^n), \boldsymbol{\epsilon}(\boldsymbol{\varphi}_{\mathfrak{m}})\rangle - \langle \boldsymbol{\mathcal{B}}\boldsymbol{\epsilon}(\boldsymbol{u}_{\mathfrak{m}}^n), \boldsymbol{\epsilon}(\boldsymbol{\varphi}_{\mathfrak{m}})\rangle . \tag{1}$$

Due to the variational inequality the contact force density fulfills the weak sign condition $\langle \boldsymbol{\lambda}_{\mathfrak{m}}^n, \boldsymbol{v}_{\mathfrak{m}} - \boldsymbol{u}_{\mathfrak{m}}^n\rangle_{-1,1} \leq 0$.
In order to investigate the contact force corresponding to the discrete setting further, we need some more notations and definitions. From now on for the ease of presentation we choose the coordinate system such that $\boldsymbol{e}_1 = \boldsymbol{\nu}$. All boundary stresses in time step n at outer or inner edges are denoted by

$$\hat{\boldsymbol{\sigma}}(\boldsymbol{u}_{\mathfrak{m}}^n) := (\boldsymbol{\mathcal{A}}\boldsymbol{\epsilon}(\delta \boldsymbol{u}_{\mathfrak{m}}^n) + \boldsymbol{\mathcal{B}}\boldsymbol{\epsilon}(\boldsymbol{u}_{\mathfrak{m}}^n))\, \boldsymbol{n}.$$

Thus, at the contact boundary in the direction of constraints we have the contact stresses $\hat{\sigma}_1(\boldsymbol{u}_{\mathfrak{m}}^n) = \boldsymbol{e}_1 \cdot (\boldsymbol{\mathcal{A}}\boldsymbol{\epsilon}(\delta \boldsymbol{u}_{\mathfrak{m}}^n) + \boldsymbol{\mathcal{B}}\boldsymbol{\epsilon}(\boldsymbol{u}_{\mathfrak{m}}^n))\, \boldsymbol{n}$. Further, we define the jump terms in the interior over a side $\mathfrak{s} \in \mathfrak{M}$ (edge in 2D, face in 3D) by $\boldsymbol{J}^I(\boldsymbol{u}_{\mathfrak{m}}^n) := (\boldsymbol{\sigma}(\boldsymbol{u}_{\mathfrak{m}}^n)|_{\mathfrak{e}_1} - \boldsymbol{\sigma}(\boldsymbol{u}_{\mathfrak{m}}^n)|_{\mathfrak{e}_2}) \cdot \boldsymbol{n}$ where $\mathfrak{e}_1$, $\mathfrak{e}_2$ are two elements sharing the side $\mathfrak{s}$ and the jump terms at the Neumann boundary $\boldsymbol{J}^N(\boldsymbol{u}_{\mathfrak{m}}^n) := \boldsymbol{\pi} - \hat{\boldsymbol{\sigma}}(\boldsymbol{u}_{\mathfrak{m}}^n)$ and at the contact boundary in tangential direction $\boldsymbol{J}_{\tan}^C(\boldsymbol{u}_{\mathfrak{m}}^n) := -\hat{\boldsymbol{\sigma}}_{\tan}(\boldsymbol{u}_{\mathfrak{m}}^n)$.
For the integration by parts we need a grid which is a union of the grids $\mathfrak{M}^n$ and $\mathfrak{M}^{n-1}$. This finest common grid denoted by $\widetilde{\mathfrak{M}}^n$ is assumed to be shape-regular. The elements of $\widetilde{\mathfrak{M}}^n$ are denoted by $\tilde{\mathfrak{e}}$, the sides by $\tilde{\mathfrak{s}}$ and the nodes by $\tilde{\boldsymbol{p}} \in \widetilde{\mathfrak{N}}_{\mathfrak{m}}^n$. There is a uniform with respect to n bound on the ratio of the diameters of elements $\mathfrak{e} \in \mathfrak{M}^n$ and $\tilde{\mathfrak{e}} \in \widetilde{\mathfrak{M}}^n$. Whenever it is clear from the context we omit the superscript n for the mesh $\mathfrak{M}$ and the set of nodes $\mathfrak{N}_{\mathfrak{m}}$.
Let $\boldsymbol{p}$ be a node belonging to the mesh $\mathfrak{M}$. We denote by ω_p the union of all elements $\mathfrak{e}$ of $\mathfrak{M}$ having the node $\boldsymbol{p}$ in common. We call the union of all sides in the interior of ω_p, not including the boundary of ω_p, by $\gamma_{p,I}$. For the intersections between Γ and $\partial\omega_p$ we distinguish between the three following types $\gamma_{p,C} := \Gamma_C \cap \partial\omega_p$, $\gamma_{p,N} := \Gamma_N \cap \partial\omega_p$ and $\gamma_{p,D} := \Gamma_D \cap \partial\omega_p$. In the same way, we define for all nodes $\tilde{\boldsymbol{p}} \in \widetilde{\mathfrak{N}}_{\mathfrak{m}}$, $\omega_{\tilde{p}}$ as the union of all elements $\tilde{\mathfrak{e}}$ of $\widetilde{\mathfrak{M}}$ having the node $\tilde{\boldsymbol{p}}$ in common. The intersection between all interior sides and $\omega_{\tilde{p}}$ is denoted by $\gamma_{\tilde{p},I}$, and respectively $\gamma_{\tilde{p},C}, \gamma_{\tilde{p},N}, \gamma_{\tilde{p},D}$. Further, we need the union of all elements $\tilde{\mathfrak{e}}$ of $\widetilde{\mathfrak{M}}$ belonging to ω_p, the patch in $\mathfrak{M}$. This area is denoted by

$$\tilde{\omega}_p := \bigcup_{\tilde{\mathfrak{e}} \subset \omega_p} \tilde{\mathfrak{e}}.$$

Accordingly, the union of all sides $\tilde{\mathfrak{s}} \in \widetilde{\mathfrak{M}}$ in $\tilde{\omega}_p$ is given by $\tilde{\gamma}_{p,I}$ and

$$\tilde{\gamma}_{p,C} := \bigcup_{\tilde{\mathfrak{s}} \subset \gamma_{p,C}} \tilde{\mathfrak{s}}, \quad \tilde{\gamma}_{p,N} := \bigcup_{\tilde{\mathfrak{s}} \subset \gamma_{p,N}} \tilde{\mathfrak{s}}, \quad \tilde{\gamma}_{p,D} := \bigcup_{\tilde{\mathfrak{s}} \subset \gamma_{p,D}} \tilde{\mathfrak{s}}.$$

Using integration by parts and the introduced notation we reformulate the discrete contact force

$$\begin{aligned} \langle \boldsymbol{\lambda}_{\mathfrak{m}}^n, \boldsymbol{\varphi}_{\mathfrak{m}} \rangle_{-1,1} = \sum_{i=1}^{d} \Bigg(& \sum_{p \in \mathfrak{N}_{\mathfrak{m}}^I} \int_{\tilde{\gamma}_{p,I}} \boldsymbol{J}^I(\boldsymbol{u}_{\mathfrak{m}}^n) \varphi_{\mathfrak{m},i}(p) \phi_p \boldsymbol{e}_i + \sum_{p \in \mathfrak{N}_{\mathfrak{m}}} \int_{\tilde{\omega}_p} \boldsymbol{f}^n \varphi_{\mathfrak{m},i}(p) \phi_p \boldsymbol{e}_i \\ & + \sum_{p \in \mathfrak{N}_{\mathfrak{m}}^{\tilde{N}}} \int_{\tilde{\gamma}_{p,N}} \boldsymbol{J}^N(\boldsymbol{u}_{\mathfrak{m}}^n) \varphi_{\mathfrak{m},i}(p) \phi_p \boldsymbol{e}_i - \sum_{p \in \mathfrak{N}_{\mathfrak{m}}^C} \int_{\tilde{\gamma}_{p,C}} \hat{\boldsymbol{\sigma}}(\boldsymbol{u}_{\mathfrak{m}}^n) \varphi_{\mathfrak{m},i}(p) \phi_p \boldsymbol{e}_i \Bigg) \end{aligned}$$

Note that for the integration by parts the mesh $\widetilde{\mathfrak{M}}$ has to be considered while we take the partition of unity with respect to the set of nodes $\mathfrak{N}_{\mathfrak{m}}$ of the mesh $\mathfrak{M}$.
Further, we define $s_p^n := \frac{\langle \lambda_{\mathfrak{m},1}^n, \phi_p \rangle_{-1,1}}{\int_{\gamma_{p,C}} \phi_p}$ which is the nodal value of the discrete contact force density obtained by lumping the boundary mass matrix. From the variational inequality the sign condition $s_p^n \geq 0$ follows. If $p \in \mathfrak{N}_{\mathfrak{m}}^C$ and $i \neq 1$ or $p \in \mathfrak{N}_{\mathfrak{m}} \backslash \mathfrak{N}_{\mathfrak{m}}^C$ we have $\langle \boldsymbol{\lambda}_{\mathfrak{m}}^n, \phi_p \boldsymbol{e}_i \rangle_{-1,1} = 0$.

2.4 Quasi-discrete contact force density

By definition the discrete contact force (1) is only a functional on the discrete space $\boldsymbol{\mathcal{H}}_{\mathfrak{m},0}$. Thus, in order to measure the error in the solution as well as in the contact forces we need an extension of the discrete contact force (1) to a functional on $\boldsymbol{\mathcal{H}}_0$. This extension is called quasi-discrete contact force and denoted by $\tilde{\boldsymbol{\lambda}}_{\mathfrak{m}}^{\tau}$. It is crucial that the quasi-discrete contact force reflects the properties of the continuous contact force $\boldsymbol{\lambda}$.
We assume that the quasi-discrete contact force is piecewise constant on each interval $(t^{n-1}, t^n]$, i.e.

$$\left\langle \tilde{\boldsymbol{\lambda}}_{\mathfrak{m}}^{\tau}, \boldsymbol{\varphi} \right\rangle_{-1,1} = \left\langle \tilde{\boldsymbol{\lambda}}_{\mathfrak{m}}^{n}, \boldsymbol{\varphi} \right\rangle_{-1,1} \quad \text{on } (t^{n-1}, t^n].$$

In the spirit of the works [9, 16, 18] we use the partition of unity in each time step n

$$\left\langle \tilde{\boldsymbol{\lambda}}_{\mathfrak{m}}^{n}, \boldsymbol{\varphi} \right\rangle_{-1,1} := \sum_{p \in \mathfrak{N}_{\mathfrak{m}}} \left\langle \tilde{\boldsymbol{\lambda}}_{\mathfrak{m},p}^{n}, \varphi_1 \phi_p \right\rangle_{-1,1}$$

which enables to handle the contributions differently depending on the contact status of the nodes. We will distinguish between so-called full-contact nodes $\boldsymbol{p} \in \mathfrak{N}_{\mathfrak{m}}^{fC}$ and semi-contact nodes $\boldsymbol{p} \in \mathfrak{N}_{\mathfrak{m}}^{sC}$.

Definition 1 (Full-contact nodes)**.** *At full-contact nodes the discrete solution fulfills the following conditions*

- $u_{\mathfrak{m},1}^n = g_{\mathfrak{m}}^n$ *on* $\tilde{\gamma}_{p,C}$
- $u_{\mathfrak{m},1}^{n-1} = g_{\mathfrak{m}}^{n-1}$ *on* $\tilde{\gamma}_{p,C}$

- $\hat{\sigma}_1(\boldsymbol{u}^n_{\mathfrak{m}}) \leq 0$ *on* $\tilde{\gamma}_{p,C}$.

At full-contact nodes the solution is in contact in the whole contact boundary patch $\tilde{\gamma}_{p,C}$ in both time steps n and $n-1$ and the contact boundary stresses, which depend also on the solutions in both time steps, fulfill the sign condition as in the continuous case. At semi-contact nodes the solution is in contact, i.e. $u^n_{\mathfrak{m},1}(\boldsymbol{p}) = g^n_{\mathfrak{m}}(\boldsymbol{p})$ in the current time step n but does not fulfill the conditions of full-contact. Compared to the works for static contact problems [16, 27] the definition of full-contact is space- and time-dependent.
In each time step n we define the quasi-discrete contact force as follows

$$\begin{aligned}\left\langle \tilde{\boldsymbol{\lambda}}^n_{\mathfrak{m}}, \boldsymbol{\varphi} \right\rangle_{-1,1} := &\sum_{p \in \mathfrak{N}^{\mathrm{sC}}_{\mathfrak{m}}} s^n_p c_p(\varphi_1) \int_{\tilde{\gamma}_{p,C}} \phi_p \\ &+ \sum_{p \in \mathfrak{N}^{\mathrm{fC}}_{\mathfrak{m}}} \left(s^n_p c_p(\varphi_1) \int_{\tilde{\gamma}_{p,C}} \phi_p - \int_{\tilde{\gamma}_{p,C}} \hat{\sigma}_1(\boldsymbol{u}^n_{\mathfrak{m}})(\varphi_1 - c_p(\varphi_1))\phi_p \right)\end{aligned} \tag{2}$$

where $c_p(\varphi_1)$ are weighted mean values. It will turn out that in order to prove reliability and efficiency we need specific choices of $c_p(\varphi_1)$ depending on the contact status of the nodes. For semi-contact nodes we use $c_p(\varphi_1) = \frac{\int_{b_p} \varphi_1 \phi_p}{\int_{b_p} \phi_p}$ with $b_p \subsetneq \gamma_{\tilde{p},C}$. b_p can be chosen as the boundary patch around $\tilde{\boldsymbol{p}} = \boldsymbol{p}$ with respect to a uniform refinement of $\widetilde{\mathfrak{M}}^n$. Thus, due to the fact that there is a uniform bound on the relation between elements of $\widetilde{\mathfrak{M}}^n$ and $\mathfrak{M}^n$ the relation between b_p and $\gamma_{p,C}$ is also bounded. For full-contact nodes we take $c_p(\varphi_1) = \frac{\int_{\bar{\mathfrak{s}}} \varphi_1 \phi_p}{\int_{\bar{\mathfrak{s}}} \phi_p}$ where $\bar{\mathfrak{s}} \subset \tilde{\gamma}_{p,C}$ fulfills

$$\frac{\int_{\bar{\mathfrak{s}}} \int_{t^{n-1}}^{t^n} \varphi_1 \phi_p}{\int_{\bar{\mathfrak{s}}} \phi_p} \geq \frac{\int_{\tilde{\mathfrak{s}}} \int_{t^{n-1}}^{t^n} \varphi_1 \phi_p}{\int_{\mathfrak{s}} \phi_p} \quad \forall \tilde{\mathfrak{s}} \subset \tilde{\gamma}_{p,C}. \tag{3}$$

We note that (3) is time-dependent as well as the definition of full-contact. However, we omit the subindex n, whenever it is clear from the context, i.e. $c_p(\varphi) = c^n_p(\varphi)$.

3 A posteriori error estimator

The aim of this section is to introduce the error estimator and to state the main theorems of efficiency and reliability. Therefore we introduce the Galerkin functional, global and local error measures and the relation between each other. The proofs of the theorems will be given in Sections 4 and 5.

3.1 Galerkin functional and error measure

A main step in the derivation of residual-type a posteriori estimators for linear problems without constraints is to establish a relation between the error measure and a linear residual, see e.g. [25] for linear elliptic and parabolic problems and [7] for linear viscoelastic problems. For contact and obstacle problems a so-called Galerkin functional replaces the linear residual, see e.g. [16, 18, 22].

For the linear viscoelastic contact problem (Problem 2) the Galerkin functional is given by

$$\begin{aligned}\langle \boldsymbol{\mathcal{G}}, \boldsymbol{\varphi}\rangle_{-1,1} &:= \langle \boldsymbol{\mathcal{A}}\boldsymbol{\epsilon}(\dot{\boldsymbol{u}} - \dot{\boldsymbol{u}}_{\mathrm{m}}^{\tau}), \boldsymbol{\epsilon}(\boldsymbol{\varphi})\rangle + \langle \boldsymbol{\mathcal{B}}\boldsymbol{\epsilon}(\boldsymbol{u} - \boldsymbol{u}_{\mathrm{m}}^{\tau}), \boldsymbol{\epsilon}(\boldsymbol{\varphi})\rangle + \left\langle \boldsymbol{\lambda} - \tilde{\boldsymbol{\lambda}}_{\mathrm{m}}^{\tau}, \boldsymbol{\varphi}\right\rangle_{-1,1} \\ &= \left\langle \tilde{\boldsymbol{f}} - \tilde{\boldsymbol{f}}^{\tau}, \boldsymbol{\varphi}\right\rangle_{-1,1} + \langle \boldsymbol{f}^{\tau}, \boldsymbol{\varphi}\rangle + \langle \boldsymbol{\pi}^{\tau}, \boldsymbol{\varphi}\rangle_{\Gamma_N} \\ &\quad - \langle \boldsymbol{\mathcal{A}}\boldsymbol{\epsilon}(\dot{\boldsymbol{u}}_{\mathrm{m}}^{\tau}), \boldsymbol{\epsilon}(\boldsymbol{\varphi})\rangle - \langle \boldsymbol{\mathcal{B}}\boldsymbol{\epsilon}(\boldsymbol{u}_{\mathrm{m}}^{\tau}), \boldsymbol{\epsilon}(\boldsymbol{\varphi})\rangle - \left\langle \tilde{\boldsymbol{\lambda}}_{\mathrm{m}}^{\tau}, \boldsymbol{\varphi}\right\rangle_{-1,1}. \end{aligned} \tag{4}$$

On each time interval $(t^{n-1}, t^n]$ we have the temporal Galerkin functional

$$\langle \boldsymbol{\mathcal{G}}_{\tau}^{n}, \boldsymbol{\varphi}\rangle_{-1,1} := \langle \boldsymbol{\mathcal{B}}\boldsymbol{\epsilon}(\boldsymbol{u}_{\mathrm{m}}^{n} - \boldsymbol{u}_{\mathrm{m}}^{\tau}), \boldsymbol{\epsilon}(\boldsymbol{\varphi})\rangle \tag{5}$$

and the spatial Galerkin functional

$$\langle \boldsymbol{\mathcal{G}}_{\mathrm{m}}^{n}, \boldsymbol{\varphi}\rangle_{-1,1} := \langle \boldsymbol{f}^{n}, \boldsymbol{\varphi}\rangle + \langle \boldsymbol{\pi}^{n}, \boldsymbol{\varphi}\rangle_{\Gamma_N} - \langle \boldsymbol{\mathcal{A}}\boldsymbol{\epsilon}(\delta \boldsymbol{u}_{\mathrm{m}}^{n}) + \boldsymbol{\mathcal{B}}\boldsymbol{\epsilon}(\boldsymbol{u}_{\mathrm{m}}^{n}), \boldsymbol{\epsilon}(\boldsymbol{\varphi})\rangle - \left\langle \tilde{\boldsymbol{\lambda}}_{\mathrm{m}}^{n}, \boldsymbol{\varphi}\right\rangle_{-1,1},$$

which is piecewise constant on each time interval, such that on $(t^{n-1}, t^n]$ we have

$$\langle \boldsymbol{\mathcal{G}}, \boldsymbol{\varphi}\rangle_{-1,1} = \langle \boldsymbol{\mathcal{G}}_{\mathrm{m}}^{n}, \boldsymbol{\varphi}\rangle_{-1,1} + \langle \boldsymbol{\mathcal{G}}_{\tau}^{n}, \boldsymbol{\varphi}\rangle_{-1,1} + \left\langle \tilde{\boldsymbol{f}} - \tilde{\boldsymbol{f}}^{n}, \boldsymbol{\varphi}\right\rangle_{-1,1}. \tag{6}$$

Let $\|\cdot\|_{L^2_{\mathcal{B}}}$ be the norm induced by the s.p.d. bilinear form $\langle \mathcal{B}(\cdot), (\cdot)\rangle$ and $\|\cdot\|_{L^2_{\mathcal{A}}}$ the norm induced by the s.p.d. bilinear form $\langle \mathcal{A}(\cdot), (\cdot)\rangle$.
In this work we will derive an a posteriori error estimator which constitutes **global** upper and lower bounds with respect to the following global error measure on the time interval I

$$\begin{aligned}&\mathrm{ErrMeasG}(\boldsymbol{u}_{\mathrm{m}}^{\tau}, \dot{\boldsymbol{u}}_{\mathrm{m}}^{\tau}, \tilde{\boldsymbol{\lambda}}_{\mathrm{m}}^{\tau}, I) := \\ &\left(\int_I \left(\sup_{\varphi \in \mathcal{H}_0} \left(\frac{\langle \boldsymbol{\mathcal{A}}\boldsymbol{\epsilon}(\dot{\boldsymbol{u}} - \dot{\boldsymbol{u}}_{\mathrm{m}}^{\tau}), \boldsymbol{\epsilon}(\boldsymbol{\varphi})\rangle + \left\langle \boldsymbol{\lambda} - \tilde{\boldsymbol{\lambda}}_{\mathrm{m}}^{\tau}, \boldsymbol{\varphi}\right\rangle_{-1,1}}{\|\nabla \boldsymbol{\varphi}\|} \right) \right)^2 \right. \\ &\left. + \|\boldsymbol{\epsilon}(\boldsymbol{u} - \boldsymbol{u}_{\mathrm{m}}^{\tau})\|^2_{L^2(I, L^2_{\mathcal{B}})} + \|\boldsymbol{\epsilon}(\boldsymbol{u} - \boldsymbol{u}_{\mathrm{m}}^{\tau})(T)\|^2_{L^2_{\mathcal{A}}} \right)^{\frac{1}{2}}\end{aligned}$$

which considers the error in the displacements, the velocities as well as in the contact force density and thus is related to the Galerkin functional (4).
Further, we derive **local** lower bounds for the spatial error in each time step n with respect to the following error measure

$$\begin{aligned}&\mathrm{ErrMeasL}(\boldsymbol{u}_{\mathrm{m}}^{n}, \dot{\boldsymbol{u}}_{\mathrm{m}}^{\tau}, \tilde{\boldsymbol{\lambda}}_{\mathrm{m}}^{n}) := \\ &\left(\left(\sup_{\varphi \in \mathcal{H}_0(\omega_p)} \left(\frac{\langle \boldsymbol{\mathcal{A}}\boldsymbol{\epsilon}(\dot{\boldsymbol{u}} - \dot{\boldsymbol{u}}_{\mathrm{m}}^{\tau}), \boldsymbol{\epsilon}(\boldsymbol{\varphi})\rangle + \left\langle \boldsymbol{\lambda} - \tilde{\boldsymbol{\lambda}}_{\mathrm{m}}^{n}, \boldsymbol{\varphi}\right\rangle_{-1,1}}{\|\nabla \boldsymbol{\varphi}\|} \right) \right)^2 + \|\boldsymbol{\epsilon}(\boldsymbol{u} - \boldsymbol{u}_{\mathrm{m}}^{n})\|^2_{L^2_{\mathcal{B}}(\omega_p)} \right)^{\frac{1}{2}}.\end{aligned}$$

Remark 1 (Relation between local and global error measure)**.** *Integrating* $\left(\mathrm{ErrMeasL}(\boldsymbol{u}_{\mathrm{m}}^{n}, \dot{\boldsymbol{u}}_{\mathrm{m}}^{\tau}, \tilde{\boldsymbol{\lambda}}_{\mathrm{m}}^{n})\right)^2$ *over the time intervall* $[t^{n-1}, t^n]$ *and comparing with* $\left(\mathrm{ErrMeasG}(\boldsymbol{u}_{\mathrm{m}}^{\tau}, \dot{\boldsymbol{u}}_{\mathrm{m}}^{\tau}, \tilde{\boldsymbol{\lambda}}_{\mathrm{m}}^{\tau}, [t^{n-1}, t^n])\right)^2$ *where* Ω *is replaced by* ω_p *the two error* *measures differ in* $\int_{t^{n-1}}^{t^n} \|\boldsymbol{\epsilon}(\boldsymbol{u}-\boldsymbol{u}_{\mathrm{m}}^{\tau})\|^2_{L^2_{\mathcal{B}}(\omega_p)}$ *and* $\int_{t^{n-1}}^{t^n} \|\boldsymbol{\epsilon}(\boldsymbol{u}-\boldsymbol{u}_{\mathrm{m}}^{n})\|^2_{L^2_{\mathcal{B}}(\omega_p)}$. *The difference can be bounded by* $\int_{t^{n-1}}^{t^n} \|\boldsymbol{\epsilon}(\boldsymbol{u}-\boldsymbol{u}_{\mathrm{m}}^{n})\|^2_{L^2_{\mathcal{B}}(\omega_p)} - \int_{t^{n-1}}^{t^n} \|\boldsymbol{\epsilon}(\boldsymbol{u}-\boldsymbol{u}_{\mathrm{m}}^{\tau})\|^2_{L^2_{\mathcal{B}}(\omega_p)} \le \int_{t^{n-1}}^{t^n} \|\boldsymbol{\epsilon}(\boldsymbol{u}_{\mathrm{m}}^{\tau}-\boldsymbol{u}_{\mathrm{m}}^{n})\|^2_{L^2_{\mathcal{B}}(\omega_p)}$. *Using the box rule for the integration shows that the difference is of order* τ^2.

The dual norm of the Galerkin functional $\boldsymbol{\mathcal{G}}$ is bounded from above by

$$\|\boldsymbol{\mathcal{G}}\|_{-1} \le \sup_{\varphi\in\mathcal{H}_0} \frac{\langle \boldsymbol{\mathcal{A}}\boldsymbol{\epsilon}(\dot{\boldsymbol{u}}-\dot{\boldsymbol{u}}_{\mathrm{m}}^{\tau}), \boldsymbol{\epsilon}(\boldsymbol{\varphi})\rangle + \left\langle \boldsymbol{\lambda}-\tilde{\boldsymbol{\lambda}}_{\mathrm{m}}^{\tau}, \boldsymbol{\varphi}\right\rangle_{-1,1}}{\|\nabla\boldsymbol{\varphi}\|} + \|\boldsymbol{\epsilon}(\boldsymbol{u}-\boldsymbol{u}_{\mathrm{m}}^{\tau})\|_{L^2_{\mathcal{B}}}$$

and respectively, after integration in time by the global error measure (3.1)

$$\|\boldsymbol{\mathcal{G}}\|_{L^2([0,T],H^{-1}])} \le \mathrm{ErrMeasG}(\boldsymbol{u}_{\mathrm{m}}^{\tau}, \dot{\boldsymbol{u}}_{\mathrm{m}}^{\tau}, \tilde{\boldsymbol{\lambda}}_{\mathrm{m}}^{\tau}, I). \tag{7}$$

The dual norm of the spatial Galerkin functional $\boldsymbol{\mathcal{G}}_{\mathrm{m}}^n$ in each time step is bounded from above by

$$\|\boldsymbol{\mathcal{G}}_{\mathrm{m}}^n\|_{-1} \le \mathrm{ErrMeasL}(\boldsymbol{u}_{\mathrm{m}}^{n}, \dot{\boldsymbol{u}}_{\mathrm{m}}^{\tau}, \tilde{\boldsymbol{\lambda}}_{\mathrm{m}}^{n}). \tag{8}$$

Lemma 1 (Abstract upper bound)**.**

$$\begin{aligned}&\Big(\mathrm{ErrMeasG}(\boldsymbol{u}_{\mathrm{m}}^{\tau}, \dot{\boldsymbol{u}}_{\mathrm{m}}^{\tau}, \tilde{\boldsymbol{\lambda}}_{\mathrm{m}}^{\tau}, [0,T])\Big)^2\\ &\lesssim \left(1+\frac{2}{C_{\mathcal{B}}}\right)\|\boldsymbol{\mathcal{G}}\|^2_{L^2([0,T];H^{-1})} + 2\|\boldsymbol{\epsilon}(\boldsymbol{u}-\boldsymbol{u}_{\mathrm{m}}^{\tau})(0)\|^2_{L^2_{\mathcal{A}}} - 4\int_0^T \left\langle \boldsymbol{\lambda}-\tilde{\boldsymbol{\lambda}}_{\mathrm{m}}^{\tau}, \boldsymbol{u}-\boldsymbol{u}_{\mathrm{m}}^{\tau}\right\rangle_{-1,1}\end{aligned} \tag{9}$$

Proof.

$$\begin{aligned}&\frac{1}{2}\frac{d}{dt}\|\boldsymbol{\epsilon}(\boldsymbol{u}-\boldsymbol{u}_{\mathrm{m}}^{\tau})\|^2_{L^2_{\mathcal{A}}} + \|\boldsymbol{\epsilon}(\boldsymbol{u}-\boldsymbol{u}_{\mathrm{m}}^{\tau})\|^2_{L^2_{\mathcal{B}}}\\ &= \langle \boldsymbol{\mathcal{A}}\partial_t\boldsymbol{\epsilon}(\boldsymbol{u}-\boldsymbol{u}_{\mathrm{m}}^{\tau}), \boldsymbol{\epsilon}(\boldsymbol{u}-\boldsymbol{u}_{\mathrm{m}}^{\tau})\rangle + \langle \boldsymbol{\mathcal{B}}\boldsymbol{\epsilon}(\boldsymbol{u}-\boldsymbol{u}_{\mathrm{m}}^{\tau}), \boldsymbol{\epsilon}(\boldsymbol{u}-\boldsymbol{u}_{\mathrm{m}}^{\tau})\rangle\\ &= \langle \boldsymbol{\mathcal{G}}, \boldsymbol{u}-\boldsymbol{u}_{\mathrm{m}}^{\tau}\rangle_{-1,1} - \left\langle \boldsymbol{\lambda}-\tilde{\boldsymbol{\lambda}}_{\mathrm{m}}^{\tau}, \boldsymbol{u}-\boldsymbol{u}_{\mathrm{m}}^{\tau}\right\rangle_{-1,1}\end{aligned}$$

Now we apply Cauchy-Schwarz, the ellipticity of $\mathcal{B}$, the scaled Young's inequality with $\epsilon = \frac{1}{2C_{\mathcal{B}}}$ where $C_{\mathcal{B}}$ is the ellipticity constant

$$\begin{aligned}\frac{1}{2}\frac{d}{dt}\|\boldsymbol{\epsilon}(\boldsymbol{u}-\boldsymbol{u}_{\mathrm{m}}^{\tau})\|^2_{L^2_{\mathcal{A}}} + \|\boldsymbol{\epsilon}(\boldsymbol{u}-\boldsymbol{u}_{\mathrm{m}}^{\tau})\|^2_{L^2_{\mathcal{B}}} &\lesssim \frac{1}{2C_{\mathcal{B}}}\|\boldsymbol{\mathcal{G}}\|^2_{-1} + \frac{C_{\mathcal{B}}}{2}\|\boldsymbol{\epsilon}(\boldsymbol{u}-\boldsymbol{u}_{\mathrm{m}}^{\tau})\|^2_{L^2} - \left\langle \boldsymbol{\lambda}-\tilde{\boldsymbol{\lambda}}_{\mathrm{m}}^{\tau}, \boldsymbol{u}-\boldsymbol{u}_{\mathrm{m}}^{\tau}\right\rangle_{-1,1}\\ &\lesssim \frac{1}{2C_{\mathcal{B}}}\|\boldsymbol{\mathcal{G}}\|^2_{-1} + \frac{1}{2}\|\boldsymbol{\epsilon}(\boldsymbol{u}-\boldsymbol{u}_{\mathrm{m}}^{\tau})\|^2_{L^2_{\mathcal{B}}} - \left\langle \boldsymbol{\lambda}-\tilde{\boldsymbol{\lambda}}_{\mathrm{m}}^{\tau}, \boldsymbol{u}-\boldsymbol{u}_{\mathrm{m}}^{\tau}\right\rangle_{-1,1}.\end{aligned}$$

Integration in time from 0 to T leads to

$$\begin{aligned}&\|\boldsymbol{\epsilon}(\boldsymbol{u}-\boldsymbol{u}_{\mathrm{m}}^{\tau})(T)\|^2_{L^2_{\mathcal{A}}} - \|\boldsymbol{\epsilon}(\boldsymbol{u}-\boldsymbol{u}_{\mathrm{m}}^{\tau})(0)\|^2_{L^2_{\mathcal{A}}} + \|\boldsymbol{\epsilon}(\boldsymbol{u}-\boldsymbol{u}_{\mathrm{m}}^{\tau})\|^2_{L^2([0,T];L^2_{\mathcal{B}})}\\ &\lesssim \frac{1}{C_{\mathcal{B}}}\|\boldsymbol{\mathcal{G}}\|^2_{L^2([0,T];H^{-1})} - 2\int_0^T \left\langle \boldsymbol{\lambda}-\tilde{\boldsymbol{\lambda}}_{\mathrm{m}}^{\tau}, \boldsymbol{u}-\boldsymbol{u}_{\mathrm{m}}^{\tau}\right\rangle_{-1,1}\end{aligned}$$

and rearranging

$$\|\boldsymbol{\epsilon}(\boldsymbol{u}-\boldsymbol{u}_{\mathrm{m}}^{\tau})(T)\|_{L^2_{\mathcal{A}}}^2+\|\boldsymbol{\epsilon}(\boldsymbol{u}-\boldsymbol{u}_{\mathrm{m}}^{\tau})\|_{L^2([0,T];L^2_{\mathcal{B}})}^2$$
$$\lesssim \frac{1}{C_{\mathcal{B}}}\|\boldsymbol{\mathcal{G}}\|_{L^2([0,T];H^{-1})}^2-2\int_0^T\left\langle\boldsymbol{\lambda}-\tilde{\boldsymbol{\lambda}}_{\mathrm{m}}^{\tau},\boldsymbol{u}-\boldsymbol{u}_{\mathrm{m}}^{\tau}\right\rangle_{-1,1}+\|\boldsymbol{\epsilon}(\boldsymbol{u}-\boldsymbol{u}_{\mathrm{m}}^{\tau})(0)\|_{L^2_{\mathcal{A}}}^2. \tag{10}$$

Furthermore, for the remaining part of the error measure, we get

$$\begin{aligned}\sup_{\boldsymbol{\varphi}\in\mathcal{H}_0}\frac{\langle\boldsymbol{\mathcal{A}}\boldsymbol{\epsilon}(\dot{\boldsymbol{u}}-\dot{\boldsymbol{u}}_{\mathrm{m}}^{\tau}),\boldsymbol{\epsilon}(\boldsymbol{\varphi})\rangle+\left\langle\boldsymbol{\lambda}-\tilde{\boldsymbol{\lambda}}_{\mathrm{m}}^{\tau},\boldsymbol{\varphi}\right\rangle_{-1,1}}{\|\nabla\boldsymbol{\varphi}\|}&\lesssim\sup_{\boldsymbol{\varphi}\in\mathcal{H}_0}\frac{\langle\boldsymbol{\mathcal{G}},\boldsymbol{\varphi}\rangle_{-1,1}}{\|\nabla\boldsymbol{\varphi}\|}+\sup_{\boldsymbol{\varphi}\in\mathcal{H}_0}\frac{\langle\boldsymbol{\mathcal{B}}\boldsymbol{\epsilon}(\boldsymbol{u}-\boldsymbol{u}_{\mathrm{m}}^{\tau}),\boldsymbol{\epsilon}(\boldsymbol{\varphi})\rangle}{\|\nabla\boldsymbol{\varphi}\|}\\&\leq\|\boldsymbol{\mathcal{G}}\|_{-1}+\|\boldsymbol{\epsilon}(\boldsymbol{u}-\boldsymbol{u}_{\mathrm{m}}^{\tau})\|_{L^2_{\mathcal{B}}}.\end{aligned}$$

Integrating in time and exploiting (10) we get

$$\int_0^T\left(\sup_{\boldsymbol{\varphi}\in\mathcal{H}_0}\frac{\langle\boldsymbol{\mathcal{A}}\boldsymbol{\epsilon}(\dot{\boldsymbol{u}}-\dot{\boldsymbol{u}}_{\mathrm{m}}^{\tau}),\boldsymbol{\epsilon}(\boldsymbol{\varphi})\rangle+\left\langle\boldsymbol{\lambda}-\tilde{\boldsymbol{\lambda}}_{\mathrm{m}}^{\tau},\boldsymbol{\varphi}\right\rangle_{-1,1}}{\|\nabla\boldsymbol{\varphi}\|}\right)^2$$
$$\lesssim(1+\frac{1}{C_{\mathcal{B}}})\|\boldsymbol{\mathcal{G}}\|_{L^2([0,T];H^{-1})}^2+\|\boldsymbol{\epsilon}(\boldsymbol{u}-\boldsymbol{u}_{\mathrm{m}}^{\tau})(0)\|_{L^2_{\mathcal{A}}}^2-2\int_0^T\left\langle\boldsymbol{\lambda}-\tilde{\boldsymbol{\lambda}}_{\mathrm{m}}^{\tau},\boldsymbol{u}-\boldsymbol{u}_{\mathrm{m}}^{\tau}\right\rangle_{-1,1} \tag{11}$$

Putting together (10) and (11) we get the result. □

3.2 Error estimator and main results

We define the estimator

$$\eta:=\left(\sum_n(\eta^n)^2\right)^{\frac{1}{2}}:=\left(\sum_n(\eta_\tau^n)^2+\tau^n(\eta_{\mathrm{m}}^n)^2\right)^{\frac{1}{2}}$$

which consists of the temporal and spatial estimators if $g=g_{\mathrm{m}}^{\tau}$. The temporal estimator is given by

$$\eta_\tau^n:=\sqrt{\frac{\tau^n}{3}}\|\boldsymbol{\epsilon}(\boldsymbol{u}_{\mathrm{m}}^n-\boldsymbol{u}_{\mathrm{m}}^{n-1})\|_{L^2_{\mathcal{B}}}$$

and the spatial estimator by

$$\eta_{\mathrm{m}}^n:=\sqrt{\sum_{k=1}^7(\eta_k^n)^2}$$

with the different contributions

$$\eta_1^n := \left(\sum_{p\in\mathfrak{N}_\mathfrak{m}} (\eta_{1,p}^n)^2 \right)^{\frac{1}{2}}, \qquad \eta_{1,p}^n := h_p \|\boldsymbol{f}^n\|_{\tilde{\omega}_p}$$

$$\eta_2^n := \left(\sum_{p\in\mathfrak{N}_\mathfrak{m}} (\eta_{2,p}^n)^2 \right)^{\frac{1}{2}}, \qquad \eta_{2,p}^n := h_p^{\frac{1}{2}} \|\boldsymbol{J}^I(\boldsymbol{u}_\mathfrak{m}^n)\|_{\tilde{\gamma}_{p,I}}$$

$$\eta_3^n := \left(\sum_{p\in\mathfrak{N}_\mathfrak{m}^{\bar{N}}} (\eta_{3,p}^n)^2 \right)^{\frac{1}{2}}, \qquad \eta_{3,p}^n := h_p^{\frac{1}{2}} \left\|\boldsymbol{J}^N(\boldsymbol{u}_\mathfrak{m}^n)\right\|_{\tilde{\gamma}_{p,N}}$$

$$\eta_4^n := \left(\sum_{p\in\mathfrak{N}_\mathfrak{m}^C} (\eta_{4,p}^n)^2 \right)^{\frac{1}{2}}, \qquad \eta_{4,p}^n := h_p^{\frac{1}{2}} \|\boldsymbol{J}_{\tan}^C(\boldsymbol{u}_\mathfrak{m}^n)\|_{\tilde{\gamma}_{p,C}}$$

$$\eta_5^n := \left(\sum_{p\in\mathfrak{N}_\mathfrak{m}^C\setminus\mathfrak{N}_\mathfrak{m}^{fC}} (\eta_{5,p}^n)^2 \right)^{\frac{1}{2}}, \quad \eta_{5,p}^n := h_p^{\frac{1}{2}} \|\hat{\sigma}_1(\boldsymbol{u}_\mathfrak{m}^n)\|_{\tilde{\gamma}_{p,C}}$$

$$\eta_6^n := \left(\sum_{p\in\mathfrak{N}_\mathfrak{m}^{sC}} (\eta_{6,p}^n)^2 \right)^{\frac{1}{2}}, \qquad \eta_{6,p}^n := \left(s_p^n \tfrac{1}{2} \textstyle\int_{b_p} (g_\mathfrak{m}^n - u_{\mathfrak{m},1}^n)\phi_p \right)^{\frac{1}{2}}$$

$$\eta_7^n := \left(\sum_{p\in\mathfrak{N}_\mathfrak{m}^{sC}} (\eta_{7,p}^n)^2 \right)^{\frac{1}{2}}, \qquad \eta_{7,p}^n := \left(s_p^n \tfrac{1}{2} \textstyle\int_{b_p} (g_\mathfrak{m}^{n-1} - u_{\mathfrak{m},1}^{n-1})\phi_p \right)^{\frac{1}{2}}$$

where h_p is the diameter of $\tilde{\omega}_p$.
If $g \neq g_\mathfrak{m}^\tau$ is not piecewise linear in space and time we get the additional estimator

$$\eta_g := \left(\sum_{k=1}^{4} \left(\sum_n \left(\eta_{g,k}^n\right)^2 \right) + \left(\eta_{g,5}\right)^2 \right)^{\frac{1}{2}}$$

which refers to the obstacle approximation and constraint violation. It consists of the following contributions

$$\eta_{g,1}^n := \left(\sum_{p\in\mathfrak{N}_\mathfrak{m}^{sC}} s_p^n \int_{t^{n-1}}^{t^n} \frac{\int_{b_p} (g - g_\mathfrak{m}^\tau)^+ \phi_p}{\int_{b_p} \phi_p} \int_{\tilde{\gamma}_p^C} \phi_p \right)^{\frac{1}{2}}$$

$$\eta_{g,2}^n := \left(\sum_{p\in\mathfrak{N}_\mathfrak{m}^{fC}} s_p^n \int_{t^{n-1}}^{t^n} \sum_{\tilde{\mathfrak{s}}\subset\tilde{\gamma}_{p,C}} \frac{\int_{\tilde{\mathfrak{s}}} |g - g_\mathfrak{m}^\tau| \phi_p}{\int_{\tilde{\mathfrak{s}}} \phi_p} \int_{\tilde{\gamma}_{p,C}} \phi_p \right)^{\frac{1}{2}}$$

$$\eta_{g,3}^n := \left(\int_{t^{n-1}}^{t^n} \|\left(u_{\mathfrak{m},1}^\tau - g\right)^+\|_{\frac{1}{2},\Gamma_C}^2 \right)^{\frac{1}{2}}$$

$$\eta_{g,4}^n := \left(\int_{t^{n-1}}^{t^n} \|\partial_t \left(u_\mathfrak{m}^\tau - g\right)^+\|_{\frac{1}{2},\Gamma_C}^2 \right)^{\frac{1}{2}}$$

$$\eta_{g,5} := \left(\|\left(u_\mathfrak{m}^\tau(0) - g(0)\right)^+\|_{\frac{1}{2},\Gamma_C}^2 + \|\left(u_\mathfrak{m}^\tau(T) - g(T)\right)^+\|_{\frac{1}{2},\Gamma_C}^2 \right)^{\frac{1}{2}}.$$

Theorem 1 (Upper bound)**.** *The estimator η provides the following upper bound of the error measure*

$$\begin{aligned}&\mathrm{ErrMeasG}(\boldsymbol{u}_\mathfrak{m}^\tau, \dot{\boldsymbol{u}}_\mathfrak{m}^\tau, \tilde{\boldsymbol{\lambda}}_\mathfrak{m}^\tau, [0,T]) \\ &\quad\lesssim \eta + \eta_g + \|\boldsymbol{\epsilon}(\boldsymbol{u} - \boldsymbol{u}_\mathfrak{m}^\tau)(0)\|_{L^2_\mathcal{A}} + \|\tilde{\boldsymbol{f}} - \tilde{\boldsymbol{f}}^\tau\|_{L^2([0,T];H^{-1})}\end{aligned}$$

In order to formulate the lower bounds we need some further definitions. Let $\bar{\boldsymbol{f}}^n$ be defined by the piecewise constant approximations of the components f_i^n and $\bar{\boldsymbol{\pi}}^n$, respectively. We define $\operatorname{osc}_p(\boldsymbol{f}^n) := \|\boldsymbol{f}^n - \bar{\boldsymbol{f}}^n\|_{\tilde{\omega}_p}$ and $\operatorname{osc}_p(\boldsymbol{\pi}^n) := \|\boldsymbol{\pi}^n - \bar{\boldsymbol{\pi}}^n\|_{\tilde{\gamma}_{p,N}}$. Further, we abbreviate $\Pi(g_{\mathfrak{m}}^\tau, u_{\mathfrak{m},1}^{n-1}, u_{\mathfrak{m},1}^n) := \nabla\left(\chi_{\tilde{\mathfrak{s}}}^n - \frac{1}{2}\left(u_{\mathfrak{m},1}^{n-1} + u_{\mathfrak{m},1}^n\right)\right)$ on $\cup_{\tilde{q}\in\tilde{\mathfrak{s}}}\omega_{\tilde{q}}$ where $\chi_{\tilde{\mathfrak{s}}}^n$ is a suitable extension of $\frac{1}{2}\left(g_{\mathfrak{m}}^{n-1} + g_{\mathfrak{m}}^n\right)$ to a finite element function. We denote the jumps over interelement sides by $[\cdot]$.

Assumption 1 (Geometric assumptions for lower bounds)**.** *In order to prove the lower bounds we assume that each boundary element with a side $\mathfrak{s}$ on Γ_C has at least one interior node and each node $\boldsymbol{p} \in \mathfrak{N}_{\mathfrak{m}}^{sC}$ belongs to at least one element which has no boundary edge.*

Theorem 2 (Global lower bound)**.** *Under the Assumption 1 and $g = g_{\mathfrak{m}}^\tau$ the estimator η^n on each time interval $[t^{n-1}, t^n]$ fulfills the global lower bound*

$$\begin{aligned}\eta^n \lesssim\ & \operatorname{ErrMeasG}(\boldsymbol{u}_{\mathfrak{m}}^\tau, \dot{\boldsymbol{u}}_{\mathfrak{m}}^\tau, \tilde{\boldsymbol{\lambda}}_{\mathfrak{m}}^\tau, [t^{n-1}, t^n]) + \|\tilde{\boldsymbol{f}} - \tilde{\boldsymbol{f}}^\tau\|_{L^2([t^{n-1},t^n],H^{-1})} \\ & + \sqrt{\tau^n}\left(\sum_{p\in\mathfrak{N}_{\mathfrak{m}}} \operatorname{osc}_p^2(\boldsymbol{f}^n) + \sum_{p\in\mathfrak{N}_{\mathfrak{m}}^{\bar{N}}} \operatorname{osc}_p^2(\boldsymbol{\pi}^n)\right. \\ & \left. + \sum_{p\in\mathfrak{N}_{\mathfrak{m}}^{sC}} \sum_{\tilde{\mathfrak{s}}\cap b_p\neq\emptyset} h_p \|[\Pi(g_{\mathfrak{m}}^\tau, u_{\mathfrak{m},1}^{n-1}, u_{\mathfrak{m},1}^n)]\|_{\cup_{\tilde{q}\in\tilde{\mathfrak{s}}}\omega_{\tilde{q}}}^2\right)^{\frac{1}{2}}\end{aligned}$$

Theorem 3 (Local lower bound)**.** *Under the Assumption 1 and $g = g_{\mathfrak{m}}^\tau$ the local spatial estimators fulfill the local lower bound*

$$\eta_{k,p}^n \lesssim \operatorname{ErrMeasL}(\boldsymbol{u}_{\mathfrak{m}}^n, \dot{\boldsymbol{u}}_{\mathfrak{m}}^\tau, \tilde{\boldsymbol{\lambda}}_{\mathfrak{m}}^n) + \operatorname{osc}_p(\boldsymbol{f}^n) + \operatorname{osc}_p(\boldsymbol{\pi}^n)$$

for $k = 1, \ldots, 5$ and

$$\begin{aligned}\eta_{k,p}^n \lesssim\ & \operatorname{ErrMeasL}(\boldsymbol{u}_{\mathfrak{m}}^n, \dot{\boldsymbol{u}}_{\mathfrak{m}}^\tau, \tilde{\boldsymbol{\lambda}}_{\mathfrak{m}}^n) \\ & + \operatorname{osc}_p(\boldsymbol{f}^n) + \operatorname{osc}_p(\boldsymbol{\pi}^n) + \sum_{\tilde{\mathfrak{s}}\cap b_p\neq\emptyset} h_p^{\frac{1}{2}} \|[\Pi(g_{\mathfrak{m}}^\tau, u_{\mathfrak{m},1}^{n-1}, u_{\mathfrak{m},1}^n)]\|_{\cup_{\tilde{q}\in\tilde{\mathfrak{s}}}\omega_{\tilde{q}}}\end{aligned}$$

for $k = 6, 7$.

Remark 2. *The definition of full-contact depending on the solutions in time steps n and $n-1$ enables to show lower bounds of η_6, η_7. In contrast, the definition of full-contact in [18] depends only on the solution in time step n. Therein the estimators comparable with η_6, η_7 have contributions from full-contact nodes. Thus, $\hat{\sigma}_1(\boldsymbol{u}_{\mathfrak{m}}^n)$ on $\gamma_{p,C}$ for $p \in \mathfrak{N}_{\mathfrak{m}}^{fC}$ is part of η_6, η_7 as it occurs in s_p but is not part of the Galerkin functional.*

Remark 3. *Although the additional term $h_p^{\frac{1}{2}} \|[\Pi(g_{\mathfrak{m}}^\tau, u_{\mathfrak{m},1}^{n-1}, u_{\mathfrak{m},1}^n)]\|_{\cup_{\tilde{q}\in\tilde{\mathfrak{s}}}\omega_{\tilde{q}}}$, which occurs only for $p \in \mathfrak{N}_{\mathfrak{m}}^{sC}$, on the right hand side of the global and local lower bounds does not depend only on the data, Theorems 2 and 3 show that the decay of η_6, η_7 is of the same order as the other estimator contributions. Further, in our numerical results, we have observed that η_6, η_7 are very small compared to the other estimator contributions.*

4 Reliability of the error estimator

In this section we give the proof of Theorem 1. Our starting point is the estimate of Lemma 1. Thus, in Section 4.1 we give an upper bound for the dual norm of the Galerkin functional $\|\boldsymbol{\mathcal{G}}\|_{L^2(0,T;H^{-1})}$ and in Section 4.2 we derive the upper bound for $-\int_0^T \left\langle \boldsymbol{\lambda} - \tilde{\boldsymbol{\lambda}}_{\mathfrak{m}}^{\tau}, \boldsymbol{u} - \boldsymbol{u}_{\mathfrak{m}}^{\tau} \right\rangle_{-1,1}$.

4.1 Upper bound of the Galerkin functional

In the following we apply integration by parts to the Galerkin functional (4) on $(t^{n-1}, t^n]$, use the partition of unity and $\langle \boldsymbol{\lambda}_{\mathfrak{m}}^n, \phi_p \boldsymbol{e}_i \rangle_{-1,1} = 0$ for all $\boldsymbol{p} \in \mathfrak{N}_{\mathfrak{m}}^C$ and $i \neq 1$ or $\boldsymbol{p} \in \mathfrak{N}_{\mathfrak{m}} \backslash \mathfrak{N}_{\mathfrak{m}}^C$. Further, we exploit the definition of the quasi-discrete contact force (2). We set $c_p(\varphi_i) = 0$ for Dirichlet nodes and $c_p(\varphi_i) := \frac{\int_{\tilde{\omega}_p} \varphi_i \phi_p}{\int_{\tilde{\omega}_p} \phi_p}$ for all nodes $\boldsymbol{p} \in \mathfrak{N}_{\mathfrak{m}}^I \cup \mathfrak{N}_{\mathfrak{m}}^N$. For this mean value and the definitions of $c_p(\varphi_i)$ for full- and semi-contact nodes defined in Section 2.4 the L^2-approximation properties hold, see [25] and [21]. Besides the L^2-approximation property, Hölders inequality is applied.

$$
\begin{aligned}
\langle \boldsymbol{\mathcal{G}}, \boldsymbol{\varphi} \rangle_{-1,1} &= \left\langle \tilde{\boldsymbol{f}} - \tilde{\boldsymbol{f}}^n, \boldsymbol{\varphi} \right\rangle_{-1,1} + \langle \boldsymbol{\mathcal{B}} \boldsymbol{\epsilon}(\boldsymbol{u}_{\mathfrak{m}}^n - \boldsymbol{u}_{\mathfrak{m}}^{\tau}), \boldsymbol{\epsilon}(\boldsymbol{\varphi}) \rangle \\
&\qquad + \langle \boldsymbol{f}^n, \boldsymbol{\varphi} \rangle + \langle \boldsymbol{\pi}^n, \boldsymbol{\varphi} \rangle_{\Gamma_N} - \langle \boldsymbol{\mathcal{A}} \boldsymbol{\epsilon}(\delta \boldsymbol{u}_{\mathfrak{m}}^n) + \boldsymbol{\mathcal{B}} \boldsymbol{\epsilon}(\boldsymbol{u}_{\mathfrak{m}}^n), \boldsymbol{\epsilon}(\boldsymbol{\varphi}) \rangle - \left\langle \tilde{\boldsymbol{\lambda}}_{\mathfrak{m}}^n, \boldsymbol{\varphi} \right\rangle_{-1,1} \\
&= \left\langle \tilde{\boldsymbol{f}} - \tilde{\boldsymbol{f}}^n, \boldsymbol{\varphi} \right\rangle_{-1,1} + \langle \boldsymbol{\mathcal{B}} \boldsymbol{\epsilon}(\boldsymbol{u}_{\mathfrak{m}}^n - \boldsymbol{u}_{\mathfrak{m}}^{\tau}), \boldsymbol{\epsilon}(\boldsymbol{\varphi}) \rangle \\
&\quad + \sum_{i=1}^d \sum_{p \in \mathfrak{N}_{\mathfrak{m}}} \Bigg(\langle f_i^n, \varphi_i \phi_p \rangle_{\tilde{\omega}_p} + \int_{\tilde{\gamma}_{p,I}} J_i^I(\boldsymbol{u}_{\mathfrak{m}}^n) \varphi_i \phi_p \\
&\quad + \int_{\tilde{\gamma}_{p,N}} J_i^N(\boldsymbol{u}_{\mathfrak{m}}^n) \varphi_i \phi_p - \int_{\tilde{\gamma}_{p,C}} \hat{\sigma}_i(\boldsymbol{u}_{\mathfrak{m}}^n) \varphi_i \phi_p \Bigg) \\
&\qquad - \left\langle \tilde{\boldsymbol{\lambda}}_{\mathfrak{m}}^n, \boldsymbol{\varphi} \right\rangle_{-1,1} \\
&= \left\langle \tilde{\boldsymbol{f}} - \tilde{\boldsymbol{f}}^n, \boldsymbol{\varphi} \right\rangle_{-1,1} + \langle \boldsymbol{\mathcal{B}} \boldsymbol{\epsilon}(\boldsymbol{u}_{\mathfrak{m}}^n - \boldsymbol{u}_{\mathfrak{m}}^{\tau}), \boldsymbol{\epsilon}(\boldsymbol{\varphi}) \rangle + \sum_{i=1}^d \sum_{p \in \mathfrak{N}_{\mathfrak{m}}} \Big(\langle f_i^n, (\varphi_i - c_p(\varphi_i)) \phi_p \rangle_{\tilde{\omega}_p} \\
&\quad + \int_{\tilde{\gamma}_{p,I}} J_i^I(\boldsymbol{u}_{\mathfrak{m}}^n)(\varphi_i - c_p(\varphi_i)) \phi_p + \int_{\tilde{\gamma}_{p,N}} J_i^N(\boldsymbol{u}_{\mathfrak{m}}^n)(\varphi_i - c_p(\varphi_i)) \phi_p \Big) \\
&\qquad - \sum_{i=2}^d \sum_{p \in \mathfrak{N}_{\mathfrak{m}}^C} \int_{\tilde{\gamma}_{p,C}} \hat{\sigma}_i(\boldsymbol{u}_{\mathfrak{m}}^n)(\varphi_i - c_p(\varphi_i)) \phi_p - \sum_{p \in \mathfrak{N}_{\mathfrak{m}} \backslash \mathfrak{N}_{\mathfrak{m}}^{fC}} \int_{\tilde{\gamma}_{p,C}} \hat{\sigma}_1(\boldsymbol{u}_{\mathfrak{m}}^n)(\varphi_1 - c_p(\varphi_1)) \phi_p \\
&\lesssim \|\tilde{\boldsymbol{f}} - \tilde{\boldsymbol{f}}^n\|_{-1} \|\boldsymbol{\nabla} \boldsymbol{\varphi}\| + \|\boldsymbol{\epsilon}(\boldsymbol{u}_{\mathfrak{m}}^n - \boldsymbol{u}_{\mathfrak{m}}^{\tau})\|_{L^2_{\mathcal{B}}} \|\boldsymbol{\nabla} \boldsymbol{\varphi}\| + \sum_{p \in \mathfrak{N}_{\mathfrak{m}}} \Big(h_p \|\boldsymbol{f}^n\|_{\tilde{\omega}_p} \|\boldsymbol{\nabla} \boldsymbol{\varphi}\|_{\tilde{\omega}_p} \\
&\qquad + h_p^{\frac{1}{2}} \|\boldsymbol{J}^I(\boldsymbol{u}_{\mathfrak{m}}^n)\|_{\tilde{\gamma}_{p,I}} \|\boldsymbol{\nabla} \boldsymbol{\varphi}\|_{\tilde{\omega}_p} + h_p^{\frac{1}{2}} \|\boldsymbol{J}^N(\boldsymbol{u}_{\mathfrak{m}}^n)\|_{\tilde{\gamma}_{p,N}} \|\boldsymbol{\nabla} \boldsymbol{\varphi}\|_{\tilde{\omega}_p} \\
&\qquad + h_p^{\frac{1}{2}} \|\boldsymbol{J}_{\tan}^C(\boldsymbol{u}_{\mathfrak{m}}^n)\|_{\tilde{\gamma}_{p,C}} \|\boldsymbol{\nabla} \boldsymbol{\varphi}\|_{\tilde{\omega}_p} \Big) + \sum_{p \in \mathfrak{N}_{\mathfrak{m}} \backslash \mathfrak{N}_{\mathfrak{m}}^{fC}} h_p^{\frac{1}{2}} \|\hat{\sigma}_1(\boldsymbol{u}_{\mathfrak{m}}^n)\|_{\tilde{\gamma}_{p,C}} \|\boldsymbol{\nabla} \varphi_1\|_{\tilde{\omega}_p}
\end{aligned}
$$

Thus, we get on each $(t^{n-1}, t^n]$

$$\|\boldsymbol{\mathcal{G}}\|_{-1} \lesssim \|\boldsymbol{\epsilon}(\boldsymbol{u}_{\mathfrak{m}}^n - \boldsymbol{u}_{\mathfrak{m}}^\tau)\|_{L^2_{\mathcal{B}}} + \left(\sum_{k=1}^{5} (\eta_k^n)^2\right)^{\frac{1}{2}} + \|\tilde{\boldsymbol{f}} - \tilde{\boldsymbol{f}}^n\|_{-1}. \tag{12}$$

Taking the square of (12) and integrating in time, we get

$$\begin{aligned} \|\boldsymbol{\mathcal{G}}\|^2_{L^2([0,T],H^{-1})} \lesssim & \sum_n \int_{t^{n-1}}^{t^n} \langle \boldsymbol{\mathcal{B}}\boldsymbol{\epsilon}(\boldsymbol{u}_{\mathfrak{m}}^n - \boldsymbol{u}_{\mathfrak{m}}^\tau), \boldsymbol{\epsilon}(\boldsymbol{u}_{\mathfrak{m}}^n - \boldsymbol{u}_{\mathfrak{m}}^\tau)\rangle \\ & + \sum_n \tau^n \sum_{k=1}^{5} (\eta_k^n)^2 + \|\tilde{\boldsymbol{f}} - \tilde{\boldsymbol{f}}^\tau\|^2_{L^2([0,T];H^{-1})}. \end{aligned} \tag{13}$$

Next, exploiting the two relations

$$\begin{aligned} \boldsymbol{u}_{\mathfrak{m}}^n - \boldsymbol{u}_{\mathfrak{m}}^\tau &= \left(\frac{t^n - t}{\tau^n}\right)(\boldsymbol{u}_{\mathfrak{m}}^n - \boldsymbol{u}_{\mathfrak{m}}^{n-1}) \\ \int_{t^{n-1}}^{t^n} \left(\frac{t^n - t}{\tau^n}\right)^\alpha dt &= \frac{\tau^n}{\alpha + 1} \end{aligned}$$

with $\alpha > 0$ we can reformulate the first sum in (13) and thus derive the estimator in time

$$\sum_n \int_{t^{n-1}}^{t^n} \langle \boldsymbol{\mathcal{B}}\boldsymbol{\epsilon}(\boldsymbol{u}_{\mathfrak{m}}^n - \boldsymbol{u}_{\mathfrak{m}}^\tau), \boldsymbol{\epsilon}(\boldsymbol{u}_{\mathfrak{m}}^n - \boldsymbol{u}_{\mathfrak{m}}^\tau)\rangle = \sum_n \frac{\tau^n}{3} \|\boldsymbol{\epsilon}(\boldsymbol{u}_{\mathfrak{m}}^n - \boldsymbol{u}_{\mathfrak{m}}^{n-1})\|^2_{L^2_{\mathcal{B}}} \tag{14}$$

such that we end up with the following upper bound of $\|\boldsymbol{\mathcal{G}}\|_{L^2([0,T],H^{-1})}$

$$\|\boldsymbol{\mathcal{G}}\|^2_{L^2([0,T],H^{-1})} \lesssim \sum_n (\eta_\tau^n)^2 + \sum_n \tau^n (\eta_{\mathfrak{m}}^n)^2 + \|\tilde{\boldsymbol{f}} - \tilde{\boldsymbol{f}}^n\|^2_{L^2([0,T];H^{-1})}. \tag{15}$$

4.2 Upper bound of $-\int_0^T \left\langle \boldsymbol{\lambda} - \tilde{\boldsymbol{\lambda}}_{\mathfrak{m}}^\tau, \boldsymbol{u} - \boldsymbol{u}_{\mathfrak{m}}^\tau \right\rangle_{-1,1}$

As $g \in W^{1,\infty}([0,T], H^{\frac{1}{2}}(\Gamma_C))$ there exists $\rho_1^\tau := \min\{u_{\mathfrak{m},1}^\tau, g\} \in W^{1,\infty}([0,T], H^{\frac{1}{2}}(\Gamma_C))$ and an extension $\rho_1^\tau \in W^{1,\infty}([0,T], H^1(\Omega))$ which follows from e.g. [28, Chapter 8] and [1, Chapter 1]. Further we set $\rho_i^\tau = u_{\mathfrak{m},i}^\tau$ for $i \neq 1$.
We recall that $\langle \lambda_i, \varphi_i\rangle_{-1,1} = 0$, $\left\langle \tilde{\lambda}_{\mathfrak{m},i}, \varphi_i \right\rangle_{-1,1} = 0$ for $i \neq 1$. Further, as $\boldsymbol{\rho}^\tau \in \boldsymbol{\mathcal{K}}$ we get

$$\begin{aligned} & -\int_0^T \left\langle \lambda_1 - \tilde{\lambda}_{\mathfrak{m},1}^\tau, u_1 - u_{\mathfrak{m},1}^\tau \right\rangle_{-1,1} \\ &= \int_0^T \left\langle \lambda_1, u_{\mathfrak{m},1}^\tau - u_1 \right\rangle_{-1,1} + \left\langle \tilde{\lambda}_{\mathfrak{m},1}^\tau, u_1 - u_{\mathfrak{m},1}^\tau \right\rangle_{-1,1} \\ &\leq \int_0^T \left\langle \lambda_1, u_{\mathfrak{m},1}^\tau - \rho_1^\tau \right\rangle_{-1,1} + \left\langle \tilde{\lambda}_{\mathfrak{m},1}^\tau, u_1 - u_{\mathfrak{m},1}^\tau \right\rangle_{-1,1} \\ &= \int_0^T \left\langle \lambda_1 - \tilde{\lambda}_{\mathfrak{m},1}^\tau, u_{\mathfrak{m},1}^\tau - \rho_1^\tau \right\rangle_{-1,1} + \left\langle \tilde{\lambda}_{\mathfrak{m},1}^\tau, u_1 - u_{\mathfrak{m},1}^\tau \right\rangle_{-1,1} + \left\langle \tilde{\lambda}_{\mathfrak{m},1}^\tau, u_{\mathfrak{m},1}^\tau - \rho_1^\tau \right\rangle_{-1,1} \end{aligned} \tag{16}$$

In order to derive a computable upper bound of the last two terms in (16) we have to distinguish between full- and semi-contact nodes according to the definition of the quasi-discrete contact force (2). We recall that the sets of nodes $\mathfrak{N}^{sC}_{\mathfrak{m}}, \mathfrak{N}^{fC}_{\mathfrak{m}}$ always refer to the mesh of the current time step n although we omit the index n. We recall that for semi-contact nodes the definition is linear. We make use of $(u^\tau_{\mathfrak{m},1} - \rho^\tau_1) = (u^\tau_{\mathfrak{m},1} - g)^+$ and of $(g - \rho^\tau_1) = (g - u^\tau_{\mathfrak{m},1})^+$ on Γ_C which follows from the definition of ρ^τ_1 and obtain

$$
\begin{aligned}
&\int_0^T \left\langle \tilde{\lambda}^\tau_{\mathfrak{m},1}, u_1 - u^\tau_{\mathfrak{m},1} \right\rangle_{-1,1} + \int_0^T \left\langle \tilde{\lambda}^\tau_{\mathfrak{m},1}, u^\tau_{\mathfrak{m},1} - \rho^\tau_1 \right\rangle_{-1,1} \\
&= \sum_n \int_{t^{n-1}}^{t^n} \left(\sum_{p \in \mathfrak{N}^{sC}_{\mathfrak{m}}} \left\langle \tilde{\lambda}^\tau_{\mathfrak{m},1}, (u_1 - \rho^\tau_1)\, \phi_p \right\rangle_{-1,1} + \sum_{p \in \mathfrak{N}^{fC}_{\mathfrak{m}}} \left\langle \tilde{\lambda}^\tau_{\mathfrak{m},1}, (u_1 - u^\tau_{\mathfrak{m},1})\, \phi_p \right\rangle_{-1,1} \right. \\
&\quad \left. + \sum_{p \in \mathfrak{N}^{fC}_{\mathfrak{m}}} \left\langle \tilde{\lambda}^\tau_{\mathfrak{m},1}, \left(u^\tau_{\mathfrak{m},1} - \rho^\tau_1\right) \phi_p \right\rangle_{-1,1} \right) \\
&\leq \sum_n \int_{t^{n-1}}^{t^n} \left(\sum_{p \in \mathfrak{N}^{sC}_{\mathfrak{m}}} s^n_p c^n_p (g - \rho^\tau_1) \int_{\tilde{\gamma}_{p,C}} \phi_p + \sum_{p \in \mathfrak{N}^{fC}_{\mathfrak{m}}} s^n_p c^n_p (g - u^\tau_{\mathfrak{m},1}) \int_{\tilde{\gamma}_{p,C}} \phi_p \right. \\
&\quad + \sum_{p \in \mathfrak{N}^{fC}_{\mathfrak{m}}} s^n_p c^n_p ((u^\tau_{\mathfrak{m},1} - g)^+) \int_{\tilde{\gamma}_{p,C}} \phi_p - \sum_{p \in \mathfrak{N}^{fC}_{\mathfrak{m}}} \left(\int_{\tilde{\gamma}_{p,C}} \hat{\sigma}_1(\boldsymbol{u}^n_{\mathfrak{m}}) \left(u^\tau_{\mathfrak{m},1} - \rho^\tau_1 - c^n_p(u^\tau_{\mathfrak{m},1} - \rho^\tau_1)\right) \phi_p \right) \\
&\quad \left. - \sum_{p \in \mathfrak{N}^{fC}_{\mathfrak{m}}} \left(\int_{\tilde{\gamma}_{p,C}} \hat{\sigma}_1(\boldsymbol{u}^n_{\mathfrak{m}}) \left(u^\tau_1 - u^\tau_{\mathfrak{m},1} - c^n_p(u^\tau_1 - u^\tau_{\mathfrak{m},1})\right) \phi_p \right) \right) \\
&\leq \sum_n \int_{t^{n-1}}^{t^n} \left(\sum_{p \in \mathfrak{N}^{sC}_{\mathfrak{m}}} s^n_p c^n_p ((g - u^\tau_{\mathfrak{m},1})^+) \int_{\tilde{\gamma}_{p,C}} \phi_p + \sum_{p \in \mathfrak{N}^{fC}_{\mathfrak{m}}} s^n_p c^n_p (g - u^\tau_{\mathfrak{m},1}) \int_{\tilde{\gamma}_{p,C}} \phi_p \right. \\
&\quad \left. + \sum_{p \in \mathfrak{N}^{fC}_{\mathfrak{m}}} s^n_p c^n_p ((u^\tau_{\mathfrak{m},1} - g)^+) \int_{\tilde{\gamma}_{p,C}} \phi_p \right).
\end{aligned}
$$

In the last line we exploited that

$$
- \sum_{p \in \mathfrak{N}^{fC}_{\mathfrak{m}}} \left(\sum_{\tilde{\mathfrak{s}} \subset \tilde{\gamma}_{p,C}} \hat{\sigma}_1(\boldsymbol{u}^n_{\mathfrak{m}})|_{\tilde{\mathfrak{s}}} \int_{t^{n-1}}^{t^n} \int_{\tilde{\mathfrak{s}}} \left(\varphi - c^n_p(\varphi)\right) \phi_p \right) \leq 0,
$$

which follows from $-\hat{\sigma}_1(\boldsymbol{u}^n_{\mathfrak{m}})|_{\tilde{\mathfrak{s}}} \geq 0$ and

$$
\int_{t^{n-1}}^{t^n} \int_{\tilde{\mathfrak{s}}} \varphi \phi_p - \int_{t^{n-1}}^{t^n} \int_{\mathfrak{s}} \phi_p \frac{\int_{\tilde{\mathfrak{s}}} \varphi \phi_p}{\int_{\tilde{\mathfrak{s}}} \phi_p} \phi_p \leq 0
$$

due to the properties of full-contact and (3). First, we consider the contributions for semi-contact nodes exploiting $\frac{\int_{\tilde{\gamma}_{p,C}} \phi_p}{\int_{b_p} \phi_p} \le C$

$$\begin{aligned}
&\sum_n \int_{t^{n-1}}^{t^n} \left(\sum_{p \in \mathfrak{N}_{\mathfrak{m}}^{sC}} s_p^n c_p^n ((g - u_{\mathfrak{m},1}^\tau)^+) \int_{\tilde{\gamma}_{p,C}} \phi_p \right) \\
&\quad \le \sum_n \int_{t^{n-1}}^{t^n} \left(\sum_{p \in \mathfrak{N}_{\mathfrak{m}}^{sC}} s_p^n c_p^n ((g - g_{\mathfrak{m}}^\tau)^+) \int_{\tilde{\gamma}_{p,C}} \phi_p \right) + \sum_n \int_{t^{n-1}}^{t^n} \left(\sum_{p \in \mathfrak{N}_{\mathfrak{m}}^{sC}} s_p^n c_p^n (g_{\mathfrak{m}}^\tau - u_{\mathfrak{m},1}^\tau) \int_{\tilde{\gamma}_{p,C}} \phi_p \right) \\
&\quad \lesssim \sum_n \left((\eta_{g,1}^n)^2 + \sum_{p \in \mathfrak{N}_{\mathfrak{m}}^{sC}} \int_{t^{n-1}}^{t^n} \int_{b_p} (g_{\mathfrak{m}}^\tau - u_{\mathfrak{m},1}^\tau) \phi_p \right) \\
&\quad = \sum_n \left((\eta_{g,1}^n)^2 + \sum_{p \in \mathfrak{N}_{\mathfrak{m}}^{sC}} s_p^n \left(\frac{\tau^n}{2} \int_{b_p} (g_{\mathfrak{m}}^n - u_{\mathfrak{m},1}^n) \phi_p + \frac{\tau^n}{2} \int_{b_p} (g_{\mathfrak{m}}^{n-1} - u_{\mathfrak{m},1}^{n-1}) \phi_p \right) \right) \\
&\quad = \sum_n \left((\eta_{g,1}^n)^2 + \tau^n (\eta_6^n)^2 + \tau^n (\eta_7^n)^2 \right). \qquad (17)
\end{aligned}$$

Second, we consider the contributions for full-contact nodes where $u_{\mathfrak{m},1}^\tau = g_{\mathfrak{m}}$

$$\begin{aligned}
&\sum_n \int_{t^{n-1}}^{t^n} \sum_{p \in \mathfrak{N}_{\mathfrak{m}}^{fC}} s_p^n c_p^n (g - u_{\mathfrak{m},1}^\tau) \int_{\tilde{\gamma}_{p,C}} \phi_p + \sum_{p \in \mathfrak{N}_{\mathfrak{m}}^{fC}} s_p^n c_p^n ((u_{\mathfrak{m},1}^\tau - g)^+) \int_{\tilde{\gamma}_{p,C}} \phi_p \\
&\le \sum_n \int_{t^{n-1}}^{t^n} \sum_{p \in \mathfrak{N}_{\mathfrak{m}}^{fC}} s_p^n \sum_{\tilde{\mathfrak{s}} \subset \gamma_{p,C}} \frac{\int_{\tilde{\mathfrak{s}}} \left((g - g_{\mathfrak{m}}^\tau)^+ + (g_{\mathfrak{m}}^\tau - g)^+ \right) \phi_p}{\int_{\tilde{\mathfrak{s}}} \phi_p} \int_{\tilde{\gamma}_{p,C}} \phi_p \\
&= \sum_n (\eta_{g,2}^n)^2. \qquad (18)
\end{aligned}$$

In remains to bound the first term in (16). To cope with our error measure we add and substract $\langle \boldsymbol{\mathcal{A}}\boldsymbol{\epsilon}(\dot{\boldsymbol{u}} - \dot{\boldsymbol{u}}_{\mathrm{m}}^{\tau}), \boldsymbol{\epsilon}(\boldsymbol{u}_{\mathrm{m}}^{\tau} - \boldsymbol{\rho}^{\tau})\rangle$.

$$
\begin{aligned}
&\int_0^T \left\langle \lambda_1 - \tilde{\lambda}_{\mathrm{m},1}^{\tau}, u_{\mathrm{m},1}^{\tau} - \rho_1^{\tau} \right\rangle_{-1,1} \\
&= \int_0^T \langle \boldsymbol{\mathcal{A}}\boldsymbol{\epsilon}(\dot{\boldsymbol{u}} - \dot{\boldsymbol{u}}_{\mathrm{m}}^{\tau}), \boldsymbol{\epsilon}(\boldsymbol{u}_{\mathrm{m}}^{\tau} - \boldsymbol{\rho}^{\tau})\rangle + \left\langle \lambda_1 - \tilde{\lambda}_{\mathrm{m},1}^{\tau}, u_{\mathrm{m},1}^{\tau} - \rho_1^{\tau} \right\rangle_{-1,1} \\
&\quad - \int_0^T \langle \boldsymbol{\mathcal{A}}\boldsymbol{\epsilon}(\dot{\boldsymbol{u}} - \dot{\boldsymbol{u}}_{\mathrm{m}}^{\tau}), \boldsymbol{\epsilon}(\boldsymbol{u}_{\mathrm{m}}^{\tau} - \boldsymbol{\rho}^{\tau})\rangle \\
&\leq \int_0^T \sup_{\boldsymbol{\varphi}\in\mathcal{H}_0} \left(\frac{\langle \boldsymbol{\mathcal{A}}\boldsymbol{\epsilon}(\dot{\boldsymbol{u}} - \dot{\boldsymbol{u}}_{\mathrm{m}}^{\tau}), \boldsymbol{\epsilon}(\boldsymbol{\varphi})\rangle + \left\langle \lambda_1 - \tilde{\lambda}_{\mathrm{m},1}^{\tau}, \varphi_1 \right\rangle_{-1,1}}{\|\boldsymbol{\nabla}\boldsymbol{\varphi}\|} \right) \|\boldsymbol{u}_{\mathrm{m}}^{\tau} - \boldsymbol{\rho}^{\tau}\|_1 \\
&\quad - \int_0^T \langle \boldsymbol{\mathcal{A}}\boldsymbol{\epsilon}(\dot{\boldsymbol{u}} - \dot{\boldsymbol{u}}_{\mathrm{m}}^{\tau}), \boldsymbol{\epsilon}(\boldsymbol{u}_{\mathrm{m}}^{\tau} - \boldsymbol{\rho}^{\tau})\rangle \\
&\lesssim \frac{1}{2}\int_0^T \left(\sup_{\boldsymbol{\varphi}\in\mathcal{H}_0} \left(\frac{\langle \boldsymbol{\mathcal{A}}\boldsymbol{\epsilon}(\dot{\boldsymbol{u}} - \dot{\boldsymbol{u}}_{\mathrm{m}}^{\tau}), \boldsymbol{\epsilon}(\boldsymbol{\varphi})\rangle + \left\langle \lambda_1 - \tilde{\lambda}_{\mathrm{m},1}^{\tau}, \varphi_1 \right\rangle_{-1,1}}{\|\boldsymbol{\nabla}\boldsymbol{\varphi}\|} \right) \right)^2 \\
&\quad + \frac{1}{2}\int_0^T \|(u_{\mathrm{m},1}^{\tau} - g)^+\|_{\frac{1}{2},\Gamma_C}^2 - \int_0^T \langle \boldsymbol{\mathcal{A}}\boldsymbol{\epsilon}(\dot{\boldsymbol{u}} - \dot{\boldsymbol{u}}_{\mathrm{m}}^{\tau}), \boldsymbol{\epsilon}(\boldsymbol{u}_{\mathrm{m}}^{\tau} - \boldsymbol{\rho}^{\tau})\rangle \\
&\leq \frac{1}{2}\int_0^T \left(\sup_{\boldsymbol{\varphi}\in\mathcal{H}_0} \left(\frac{\langle \boldsymbol{\mathcal{A}}\boldsymbol{\epsilon}(\dot{\boldsymbol{u}} - \dot{\boldsymbol{u}}_{\mathrm{m}}^{\tau}), \boldsymbol{\epsilon}(\boldsymbol{\varphi})\rangle + \left\langle \lambda_1 - \tilde{\lambda}_{\mathrm{m},1}^{\tau}, \varphi_1 \right\rangle_{-1,1}}{\|\boldsymbol{\nabla}\boldsymbol{\varphi}\|} \right) \right)^2 \\
&\quad + \frac{1}{2}\sum_n (\eta_{g,3}^n)^2 - \int_0^T \langle \boldsymbol{\mathcal{A}}\boldsymbol{\epsilon}(\dot{\boldsymbol{u}} - \dot{\boldsymbol{u}}_{\mathrm{m}}^{\tau}), \boldsymbol{\epsilon}(\boldsymbol{u}_{\mathrm{m}}^{\tau} - \boldsymbol{\rho}^{\tau})\rangle \qquad (19)
\end{aligned}
$$

As the first term in (19) is part of the error measure, the second one is an estimator contribution, it remains to bound the last one. Therefore we use integration by parts in time.

$$
\begin{aligned}
&- \int_0^T \langle \boldsymbol{\mathcal{A}}\boldsymbol{\epsilon}(\dot{\boldsymbol{u}} - \dot{\boldsymbol{u}}_{\mathrm{m}}^{\tau}), \boldsymbol{\epsilon}(\boldsymbol{u}_{\mathrm{m}}^{\tau} - \boldsymbol{\rho}^{\tau})\rangle \\
&= - \langle \boldsymbol{\mathcal{A}}\boldsymbol{\epsilon}(\boldsymbol{u} - \boldsymbol{u}_{\mathrm{m}}^{\tau}), \boldsymbol{\epsilon}(\boldsymbol{u}_{\mathrm{m}}^{\tau} - \boldsymbol{\rho}^{\tau})\rangle |_0^T + \int_0^T \langle \boldsymbol{\mathcal{A}}\boldsymbol{\epsilon}(\boldsymbol{u} - \boldsymbol{u}_{\mathrm{m}}^{\tau}), \boldsymbol{\epsilon}(\dot{\boldsymbol{u}}_{\mathrm{m}}^{\tau} - \dot{\boldsymbol{\rho}}^{\tau})\rangle \\
&\lesssim \frac{1}{2}\|\boldsymbol{\epsilon}(\boldsymbol{u} - \boldsymbol{u}_{\mathrm{m}}^{\tau})(T)\|_{L^2_{\mathcal{A}}}^2 + \frac{1}{2}\|(u_{\mathrm{m},1}^{\tau} - g)^+(T)\|_{\frac{1}{2},\Gamma_C}^2 + \frac{1}{2}\|\boldsymbol{\epsilon}(\boldsymbol{u} - \boldsymbol{u}_{\mathrm{m}}^{\tau})(0)\|_{L^2_{\mathcal{A}}}^2 \\
&\quad + \frac{1}{2}\|(u_{\mathrm{m},1}^{\tau} - g)^+(0)\|_{\frac{1}{2},\Gamma_C}^2 + \frac{1}{2}\int_0^T \|\boldsymbol{\epsilon}(\boldsymbol{u} - \boldsymbol{u}_{\mathrm{m}}^{\tau})\|_{L^2_{\mathcal{A}}}^2 + \frac{1}{2}\int_0^T \|\partial_t \left((u_{\mathrm{m},1}^{\tau} - g)^+\right)\|_{\frac{1}{2},\Gamma_C}^2 \\
&\lesssim \frac{1}{2}\|\boldsymbol{\epsilon}(\boldsymbol{u} - \boldsymbol{u}_{\mathrm{m}}^{\tau})(T)\|_{L^2_{\mathcal{A}}}^2 + \frac{1}{2}\|\boldsymbol{\epsilon}(\boldsymbol{u} - \boldsymbol{u}_{\mathrm{m}}^{\tau})(0)\|_{L^2_{\mathcal{A}}}^2 \\
&\quad + (\eta_{g,5})^2 + \frac{1}{2}\|\boldsymbol{\epsilon}(\boldsymbol{u} - \boldsymbol{u}_{\mathrm{m}}^{\tau})\|_{L^2([0,T];L^2_{\mathcal{B}})}^2 + \sum_n (\eta_{g,4}^n)^2 \qquad (20)
\end{aligned}
$$

Putting together (17), (18), (19) and (20) we get

$$
\begin{aligned}
&-\int_0^T \left\langle \lambda_1 - \tilde{\lambda}^\tau_{\mathtt{m},1}, u_1 - u^\tau_{\mathtt{m},1} \right\rangle_{-1,1} \\
&\lesssim \frac{1}{2}\|\boldsymbol{\epsilon}(\boldsymbol{u}-\boldsymbol{u}^\tau_{\mathtt{m}})(T)\|^2_{L^2_{\mathcal{A}}} + \frac{1}{2}\|\boldsymbol{\epsilon}(\boldsymbol{u}-\boldsymbol{u}^\tau_{\mathtt{m}})(0)\|^2_{L^2_{\mathcal{A}}} + \frac{1}{2}\|\boldsymbol{\epsilon}(\boldsymbol{u}-\boldsymbol{u}^\tau_{\mathtt{m}})\|^2_{L^2([0,T];L^2_{\mathcal{B}})} \\
&\quad + \frac{1}{2}\int_0^T \left(\sup_{\varphi\in\mathcal{H}_0} \left(\frac{\langle \boldsymbol{\mathcal{A}}\boldsymbol{\epsilon}(\dot{\boldsymbol{u}} - \dot{\boldsymbol{u}}^\tau_{\mathtt{m}}), \boldsymbol{\epsilon}(\boldsymbol{\varphi})\rangle + \left\langle \lambda_1 - \tilde{\lambda}^\tau_{\mathtt{m},1}, \varphi_1 \right\rangle_{-1,1}}{\|\boldsymbol{\nabla}\boldsymbol{\varphi}\|} \right)\right)^2 \\
&\quad + \sum_n \left(\tau^n(\eta^n_6)^2 + \tau^n(\eta^n_7)^2\right) + \sum_n \left((\eta^n_{g,1})^2 + (\eta^n_{g,2})^2 + (\eta^n_{g,3})^2 + (\eta^n_{g,4})^2\right) + (\eta_{g,5})^2
\end{aligned}
$$

Combining this result with Lemma 1 and estimate (15) we have proven Theorem 1.

Remark 4 (Upper bound for discrete gap function)**.** *Under the assumption that the gap function is discrete $g = g^\tau_{\mathtt{m}}$ and thus we can define $\rho^\tau_1 := \min\{u^\tau_{\mathtt{m},1}, g\} = u^\tau_{\mathtt{m},1}$ on Ω all estimator contributions $\eta^n_{g,k}$ vanish.*

5 Lower bound of the error estimator

In this section we give the proof of Theorems 2 and 3, i.e. the lower bound in terms of the contributions η^n_k for $k = 1, ..., 7$. We note that no lower bounds are given for the data-dependent estimator contribution η_g.

From (7) we know that $\|\boldsymbol{\mathcal{G}}\|^2_{L^2([t^{n-1},t^n],H^{-1})}$ is bounded by the error measure $\mathrm{ErrMeasG}(\boldsymbol{u}^\tau_{\mathtt{m}}, \dot{\boldsymbol{u}}^\tau_{\mathtt{m}}, \tilde{\boldsymbol{\lambda}}^\tau_{\mathtt{m}}, I)$ and from (8) that $\|\boldsymbol{\mathcal{G}}^n_{\mathtt{m}}\|_{-1}$ is bounded by the local error measure $\mathrm{ErrMeasL}(\boldsymbol{u}^n_{\mathtt{m}}, \dot{\boldsymbol{u}}^\tau_{\mathtt{m}}, \tilde{\boldsymbol{\lambda}}^n_{\mathtt{m}})$. Thus, in order to derive a lower bound we show that the estimator contributions are bounded by the dual norm of the Galerkin functional.

We start with a bound of the estimator in time η^n_τ by the dual norm of $\boldsymbol{\mathcal{G}}^n_\tau$. Next, we give local bounds of the standard estimator contributions in space η^n_k for $k = 1, ..., 4$ by the dual norm of $\boldsymbol{\mathcal{G}}^n_{\mathtt{m}}$. Then, we consider the estimator contributions related to the contact boundary η^n_k for $k = 5, .., 7$. Finally, we bound the sum of the norms $\|\boldsymbol{\mathcal{G}}^n_\tau\|^2_{L^2([t^{n-1},t^n],H^{-1})}$, $\|\boldsymbol{\mathcal{G}}^n_{\mathtt{m}}\|^2_{L^2([t^{n-1},t^n],H^{-1})}$ by the norm of the sum $\|\boldsymbol{\mathcal{G}}\|^2_{L^2([t^{n-1},t^n],H^{-1})}$ plus data oscillation following [25, Lemma 6.3] (or [25, Lemma 3.53], respectively).

5.1 Bound of the estimator in time

In this section we give a bound of the estimator in time η^n_τ by $\|\boldsymbol{\mathcal{G}}^n_\tau\|^2_{L^2([t^{n-1},t^n],H^{-1})}$ which is global in space but local in time. The upper bound for the estimator in time η^n_τ follows from (14), the definition of the temporal Galerkin functional

5) and Hölder's inequality

$$\begin{aligned}\frac{\tau^n}{3}\|\boldsymbol{\epsilon}(\boldsymbol{u}_{\mathfrak{m}}^n-\boldsymbol{u}_{\mathfrak{m}}^{n-1})\|_{L^2_{\mathcal{B}}}^2 &= \int_{t^{n-1}}^{t^n}\langle\boldsymbol{\mathcal{B}}\boldsymbol{\epsilon}(\boldsymbol{u}_{\mathfrak{m}}^n-\boldsymbol{u}_{\mathfrak{m}}^\tau),\boldsymbol{\epsilon}(\boldsymbol{u}_{\mathfrak{m}}^n-\boldsymbol{u}_{\mathfrak{m}}^\tau)\rangle\\ &= \int_{t^{n-1}}^{t^n}\langle\boldsymbol{\mathcal{G}}_\tau^n,\boldsymbol{u}_{\mathfrak{m}}^n-\boldsymbol{u}_{\mathfrak{m}}^\tau\rangle_{-1,1}\\ &\lesssim \left(\int_{t^{n-1}}^{t^n}\|\boldsymbol{\mathcal{G}}_\tau^n\|_{-1}^2\right)^{\frac{1}{2}}\left(\frac{\tau^n}{3}\right)^{\frac{1}{2}}\|\boldsymbol{\epsilon}(\boldsymbol{u}_{\mathfrak{m}}^n-\boldsymbol{u}_{\mathfrak{m}}^{n-1})\|_{L^2_{\mathcal{B}}}\end{aligned}$$

and therewith we get

$$\eta_\tau^n \lesssim \left(\int_{t^{n-1}}^{t^n}\|\boldsymbol{\mathcal{G}}_\tau^n\|_{-1}^2\right)^{\frac{1}{2}} = \|\boldsymbol{\mathcal{G}}_\tau^n\|_{L^2([t^{n-1},t^n],H^{-1})}. \tag{21}$$

5.2 Local bound in space of $\eta_1^n,\dots,\eta_4^n$

To prove that η_k^n, $k=1,\dots,4$ are bounded from above by $\|\boldsymbol{\mathcal{G}}_{\mathfrak{m}}^n\|_{-1,\omega_p}$ and respectively by the local error measure (plus data oscillation) we proceed as in [26]. The properties of the element bubble functions $\Psi_{\tilde{\mathfrak{e}}}$ and side bubble functions $\Psi_{\tilde{\mathfrak{s}}}$, see e.g. [25] are used. Due to the definition of the quasi-discrete contact force density, especially of the mean values $c_p(\varphi_1)$ for all $p\in\mathfrak{N}_{\mathfrak{m}}^C$, it follows that $c_p(\Psi_{\mathfrak{e}})=0$ and $c_p(\Psi_{\mathfrak{s}})=0$ for interior and Neumann boundary sides. Thus, it is obvious that the proof follows as in the case of a linear elliptic problem where $\boldsymbol{\mathcal{G}}_{\mathfrak{m}}$ replaces the linear residual and we get

$$\sum_{k=1}^4\eta_{k,p}^n \lesssim \|\boldsymbol{\mathcal{G}}_{\mathfrak{m}}^n\|_{-1,\tilde{\omega}_p}+\mathrm{osc}_p(\boldsymbol{f}^n)+\mathrm{osc}_p(\boldsymbol{\pi}^n). \tag{22}$$

Together with (8) we have a local bound

$$\sum_{k=1}^4\eta_{k,p}^n \lesssim \mathrm{ErrMeasL}(\boldsymbol{u}_{\mathfrak{m}}^n,\dot{\boldsymbol{u}}_{\mathfrak{m}}^\tau,\tilde{\boldsymbol{\lambda}}_{\mathfrak{m}}^n)+\mathrm{osc}_p(\boldsymbol{f}^n)+\mathrm{osc}_p(\boldsymbol{\pi}^n). \tag{23}$$

5.3 Local bound in space of η_5^n

In order to give a bound of η_5^n by means of the dual norm of the spatial Galerkin functional $\|\boldsymbol{\mathcal{G}}_{\mathfrak{m}}^n\|_{-1,\omega_p}$, the bubble functions have to be adapted appropriately in the spirit of [16, Section 5.1]. Let $\bar{\boldsymbol{p}}\in\mathfrak{N}_{\mathfrak{m}}^C\backslash\mathfrak{N}_{\mathfrak{m}}^{fC}$ be an arbitrary but fixed node and $\tilde{\mathfrak{s}}$ be a side of $\widetilde{\mathfrak{M}}$ with $\tilde{\mathfrak{s}}\cap b_{\bar{p}}\neq\emptyset$. Taking for example the bubble function $\Psi_{\tilde{\mathfrak{s}}}$ we get

$$\begin{aligned}&\sum_{p\in\mathfrak{N}_{\mathfrak{m}}\backslash\mathfrak{N}_{\mathfrak{m}}^{fC}}\int_{\tilde{\mathfrak{s}}}\hat{\sigma}_1(\boldsymbol{u}_{\mathfrak{m}}^n)\Psi_{\tilde{\mathfrak{s}}}\phi_p\\ =\quad & -\langle\boldsymbol{\mathcal{G}}_{\mathfrak{m}}^n,\Psi_{\tilde{\mathfrak{s}}}\boldsymbol{e}_1\rangle_{-1,1}+\sum_{p\in\mathfrak{N}_{\mathfrak{m}}}\langle f_1^n,\Psi_{\tilde{\mathfrak{s}}}\phi_p\rangle_{\omega_{\tilde{s}}}\\ &-\sum_{p\in\mathfrak{N}_{\mathfrak{m}}^C}s_p^n c_p(\Psi_{\tilde{\mathfrak{s}}})\int_{\tilde{\gamma}_{p,C}}\phi_p+\sum_{p\in\mathfrak{N}^{fC}}\hat{\sigma}_1(\boldsymbol{u}_{\mathfrak{m}}^n)c_p(\Psi_{\tilde{\mathfrak{s}}})\phi_p,\end{aligned} \tag{24}$$

i.e. the direct relation between the Galerkin functional and $\hat{\sigma}_1(\boldsymbol{u}_{\mathfrak{m}}^n)$ is disturbed by additional contributions with the factor $c_p(\Psi_{\tilde{\mathfrak{s}}})$. Thus, we will replace $\Psi_{\tilde{\mathfrak{s}}}$ by a suitable function $\theta_{\tilde{\mathfrak{s}}}$ such that $c_p(\theta_{\tilde{\mathfrak{s}}}) = 0$ for all semi- and full-contact nodes. Let $\mathfrak{s}$ be a side of $\mathfrak{M}$ with $\tilde{\mathfrak{s}} \subseteq \mathfrak{s}$ and denote by $\boldsymbol{p}_i$ the nodes of $\mathfrak{s}$ which are in $\mathfrak{N}_{\mathfrak{m}} \backslash \mathfrak{N}_{\mathfrak{m}}^{fC}$. We note that $\boldsymbol{p} = \tilde{\boldsymbol{p}}$ as the node belongs to $\mathfrak{M}$ as well as to $\widetilde{\mathfrak{M}}$ and b_p is the boundary patch around $\boldsymbol{p}$ with respect to a uniform refinement of $\gamma_{\tilde{p},C}$. Further, for the function $\theta_{\tilde{\mathfrak{s}}}$ we make the ansatz that it is a linear combination of all bubble functions with respect to the refined mesh. The coefficients of the linear combination are determined such that

1. $\int_{\tilde{\mathfrak{s}}} 1 = \sum_{p_i \in \mathfrak{N}_{\mathfrak{m}} \backslash \mathfrak{N}_{\mathfrak{m}}^{fC}} \int_{\tilde{\mathfrak{s}}} \theta_{\tilde{\mathfrak{s}}} \phi_{p_i}$
2. $\int_{\tilde{\mathfrak{s}} \cap b_{p_i}} \theta_{\tilde{\mathfrak{s}}} \phi_{p_i} = 0$ for all semi-contact nodes
3. $\int_{\tilde{\mathfrak{s}}} \theta_{\tilde{\mathfrak{s}}} \phi_{p_i} = 0$ for all full-contact nodes with $\bar{\mathfrak{s}} = \tilde{\mathfrak{s}}$

If $\tilde{\mathfrak{s}} = \mathfrak{s}$ the construction of $\theta_{\tilde{\mathfrak{s}}}$ is the same as in [16, Section 5.1]. As $\bar{\boldsymbol{p}}$ is not a full-contact node the third condition will not be required for all $\boldsymbol{p}_i$ and thus, there is at least one contribution in the right hand side of the first condition. At this point the special choice of $c_p(\varphi)$ as mean value on b_p with $b_p \cap \tilde{\mathfrak{s}} \neq \tilde{\mathfrak{s}}$ for semi-contact nodes becomes clear because if $b_p \cap \tilde{\mathfrak{s}} = \tilde{\mathfrak{s}}$ the first condition would contradict the second condition.
If $\tilde{\mathfrak{s}} \subsetneq \mathfrak{s}$ we have $\tilde{\mathfrak{s}} \cap b_{p_i} = \emptyset$ for some or even all p_i. In the case $\tilde{\mathfrak{s}} \cap b_{p_i} = \emptyset$ the second condition is fulfilled trivially.
As we assumed that the elements are simplices, $\hat{\sigma}_1(\boldsymbol{u}_{\mathfrak{m}}^n)$ is constant on $\tilde{\mathfrak{s}}$ and thus with the last conditions, $c_p(\theta_{\tilde{\mathfrak{s}}}) = c_p(\hat{\sigma}_1(\boldsymbol{u}_{\mathfrak{m}}^n)\theta_{\tilde{\mathfrak{s}}}) = 0$. Together with the first condition and (24) we get

$$\begin{aligned} \|\hat{\sigma}_1(\boldsymbol{u}_{\mathfrak{m}}^n)\|_{\tilde{\mathfrak{s}}}^2 &= \sum_{p \in \mathfrak{N}_{\mathfrak{m}} \backslash \mathfrak{N}_{\mathfrak{m}}^{fC}} \int_{\tilde{\mathfrak{s}}} \hat{\sigma}_1(\boldsymbol{u}_{\mathfrak{m}}^n) \hat{\sigma}_1(\boldsymbol{u}_{\mathfrak{m}}^n) \theta_{\tilde{\mathfrak{s}}} \phi_p \\ &\lesssim \|\boldsymbol{\mathcal{G}}_{\mathfrak{m}}^n\|_{-1,\tilde{\omega}_p} h_p^{-\frac{1}{2}} \|\hat{\sigma}_1(\boldsymbol{u}_{\mathfrak{m}}^n)\|_{\tilde{\mathfrak{s}}} + h_p^{\frac{1}{2}} \|f_1^n\|_{\tilde{\omega}_p} \|\hat{\sigma}_1(\boldsymbol{u}_{\mathfrak{m}}^n)\|_{\tilde{\mathfrak{s}}}. \end{aligned} \tag{25}$$

Here, we used the properties of the bubble functions on the subgrid of $\widetilde{\mathfrak{M}}^n$ which constitute by linear combination $\theta_{\tilde{\mathfrak{s}}}$. Dividing by $h_p^{-\frac{1}{2}} \|\hat{\sigma}_1(\boldsymbol{u}_{\mathfrak{m}}^n)\|_{\tilde{\mathfrak{s}}}$, using the triangle inequality and exploiting the results (23) and (8) we get

$$\eta_{5,p}^n \lesssim \mathrm{ErrMeasL}(\boldsymbol{u}_{\mathfrak{m}}^n, \dot{\boldsymbol{u}}_{\mathfrak{m}}^\tau, \tilde{\boldsymbol{\lambda}}_{\mathfrak{m}}^n) + \mathrm{osc}_p(\boldsymbol{f}^n) + \mathrm{osc}_p(\boldsymbol{\pi}^n). \tag{26}$$

5.4 Local bound in space of η_6, η_7

Summing up the two error estimator contributions we get

$$\begin{aligned} (\eta_{6,p}^n)^2 + (\eta_{7,p}^n)^2 &= s_p^n \int_{b_p} \frac{1}{2}(g_{\mathfrak{m}}^n - u_{\mathfrak{m},1}^n)\phi_p + \frac{1}{2}(g_{\mathfrak{m}}^n - u_{\mathfrak{m},1}^{n-1})\phi_p \\ &= s_p^n \int_{b_p} (\chi_{\tilde{p}}^n - w_{\mathfrak{m},1}^n)\phi_p \end{aligned}$$

where we set $\chi_{\tilde{p}}^n := \frac{1}{2}(g_{\mathfrak{m}}^n + g_{\mathfrak{m}}^{n-1})$ and $w_{\mathfrak{m},1}^n := \frac{1}{2}(u_{\mathfrak{m},1}^n + u_{\mathfrak{m},1}^{n-1})$. If $s_p^n = 0$ or $(\chi_{\tilde{p}}^n - w_{\mathfrak{m},1}^n) = 0$ on b_p we have $s_p^n \int_{b_p} (\chi_{\tilde{p}}^n - w_{\mathfrak{m},1}^n)\phi_p = 0$. Therefore, we assume

$s_p^n > 0$ and $(\chi_{\tilde{p}}^n - w_{\mathfrak{m},1}^n)(q) > 0$ for at least one node, i.e. $(g_{\mathfrak{m}}^n - u_{\mathfrak{m},1}^n)(\boldsymbol{q}) > 0$ for one node $\boldsymbol{q} \in \mathfrak{N}_{\mathfrak{m}}^n$ or $(g_{\mathfrak{m}}^{n-1} - u_{\mathfrak{m}}^{n-1})(\boldsymbol{q}) > 0$ for one node $\boldsymbol{q} \in \mathfrak{N}_{\mathfrak{m}}^{n-1}$. We note that $\boldsymbol{p}$ belongs to $\mathfrak{M}$ as well as to $\widetilde{\mathfrak{M}}$.
In the case that $(\chi_{\tilde{p}}^n - w_{\mathfrak{m},1}^n)(\boldsymbol{p}) = 0$ we can derive an upper bound as in [16, Section 5.2]. But as $s_p^n > 0$ implies $(g_{\mathfrak{m}}^n - u_{\mathfrak{m},1}^n)(\boldsymbol{p}) = 0$ but not necessarily $(g_{\mathfrak{m}}^{n-1} - u_{\mathfrak{m},1}^{n-1})(\boldsymbol{p}) = 0$, we have to consider the case that $(\chi_{\tilde{p}}^n - w_{\mathfrak{m},1}^n)(\boldsymbol{p}) > 0$, too. In order to derive an upper bound of

$$\int_{b_p} (\chi_{\tilde{p}}^n - w_{\mathfrak{m},1}^n)\phi_p = \sum_{\tilde{\mathfrak{s}} \subset \gamma_{\tilde{p},C}} \int_{\tilde{\mathfrak{s}} \cap b_p} (\chi_{\tilde{\mathfrak{s}}}^n - w_{\mathfrak{m},1}^n)\phi_p$$

we consider the integral over each side independently where $\chi_{\tilde{\mathfrak{s}}}^n = \chi_{\tilde{p}}^n|_{\tilde{\mathfrak{s}}}$. For each side $\tilde{\mathfrak{s}} \cap b_p \neq \emptyset$ belonging to an element $\tilde{\mathfrak{e}}$, we choose a node $\boldsymbol{q}^*$ fulfilling $(\chi_{\tilde{\mathfrak{s}}}^n - w_{\mathfrak{m},1}^n)(\boldsymbol{q}^*) > (\chi_{\tilde{\mathfrak{s}}}^n - w_{\mathfrak{m},1}^n)(\boldsymbol{q})$ for all $\boldsymbol{q}$ on $\tilde{\mathfrak{s}}$. Further, we define $\boldsymbol{\tau}^*$ the unit vector pointing from a node $\boldsymbol{q}$ of $\tilde{\mathfrak{s}}$ to $\boldsymbol{q}^*$ such that

$$\nabla|_{\tilde{\mathfrak{e}}}(\chi_{\tilde{\mathfrak{s}}}^n - w_{\mathfrak{m},1}^n) \cdot \boldsymbol{\tau}^* > 0.$$

First, we consider the two-dimensional case. Due to the Assumption 1 we can choose a neighbouring node $\boldsymbol{z}_1$ in the interior belonging to another element $\hat{\mathfrak{e}}$. We define an extension of $\chi_{\tilde{\mathfrak{s}}}^n$ to a finite element function $\bar{\chi}_{\tilde{\mathfrak{s}}}^n$ in the interior of the domain with $\bar{\chi}_{\tilde{\mathfrak{s}}}^n(\boldsymbol{z}_1) := w_{\mathfrak{m},1}^n(\boldsymbol{z}_1)$ such that

$$\begin{aligned}(\bar{\chi}_{\tilde{\mathfrak{s}}}^n - w_{\mathfrak{m},1}^n)(\boldsymbol{q}^*) &= \underbrace{(\bar{\chi}_{\tilde{\mathfrak{s}}}^n - w_{\mathfrak{m},1}^n)(\boldsymbol{z}_1)}_{=0} + (\boldsymbol{q}^* - \boldsymbol{z}_1)\nabla|_{\hat{\mathfrak{e}}}(\bar{\chi}_{\tilde{\mathfrak{s}}}^n - w_{\mathfrak{m},1}^n) \\ &\lesssim h_p \underbrace{\nabla|_{\hat{\mathfrak{e}}}(\bar{\chi}_{\tilde{\mathfrak{s}}}^n - w_{\mathfrak{m},1}^n) \cdot \boldsymbol{\tau}_1}_{>0} \end{aligned} \tag{27}$$

where $\boldsymbol{\tau}_1$ is the unit vector pointing from $\boldsymbol{z}_1$ to $\boldsymbol{q}^*$. Further, we can choose another neighbouring node $\boldsymbol{z}_2$ in the interior belonging to the element $\tilde{\mathfrak{e}}$ and define the discrete extension $\bar{\chi}_{\tilde{\mathfrak{s}}}^n$ such that $(\bar{\chi}_{\tilde{\mathfrak{s}}}^n - w_{\mathfrak{m},1}^n)(\boldsymbol{z}_2) = (\bar{\chi}_{\tilde{\mathfrak{s}}}^n - w_{\mathfrak{m},1}^n)(\boldsymbol{q}^*)$. Thus,

$$\pm\boldsymbol{\tau}_2 \nabla|_{\tilde{\mathfrak{e}}}(\bar{\chi}_{\tilde{\mathfrak{s}}}^n - w_{\mathfrak{m},1}^n) = 0 \tag{28}$$

holds for $\boldsymbol{\tau}_2$ pointing from $\boldsymbol{z}_2$ to $\boldsymbol{q}^*$. The line given by $\boldsymbol{q}^*$ and the vector $\boldsymbol{\tau}_2$ divides the plane into half-planes with $\boldsymbol{\tau}^*$ and $-\boldsymbol{\tau}_1$ on one side and $\boldsymbol{\tau}_1$ on the other side. Therefore,

$$-\boldsymbol{\tau}_1 = \alpha\boldsymbol{\tau}_2 + \beta\boldsymbol{\tau}^* \tag{29}$$

with $\beta > 0$ and α arbitrary, see Figure 1. Combining (27, 28, 29) we get

$$\nabla|_{\tilde{\mathfrak{e}}}(\bar{\chi}_{\tilde{\mathfrak{s}}}^n - w_{\mathfrak{m},1}^n)(-\boldsymbol{\tau}_1) \geq 0, \tag{30}$$

such that

$$(\bar{\chi}_{\tilde{\mathfrak{s}}}^n - w_{\mathfrak{m},1}^n)(\boldsymbol{q}^*) \lesssim h_p \left(\nabla|_{\hat{\mathfrak{e}}}(\bar{\chi}_{\tilde{\mathfrak{s}}}^n - w_{\mathfrak{m},1}^n) - \nabla|_{\tilde{\mathfrak{e}}}(\bar{\chi}_{\tilde{\mathfrak{s}}}^n - w_{\mathfrak{m},1}^n)\right) \cdot \boldsymbol{\tau}_1. \tag{31}$$

In the three-dimensional case we can proceed almost in the same way. The interior node of $\tilde{\mathfrak{e}}$ will be denoted by $\boldsymbol{z}_3$ and we define a discrete extension of $\chi_{\tilde{\mathfrak{s}}}^n$ to $\bar{\chi}_{\tilde{\mathfrak{s}}}^n$ to the interior of the domain by $(\bar{\chi}_{\tilde{\mathfrak{s}}}^n - w_{\mathfrak{m},1}^n)(\boldsymbol{z}_3) = (\bar{\chi}_{\tilde{\mathfrak{s}}}^n - w_{\mathfrak{m},1}^n)(\boldsymbol{q}^*)$. With $\boldsymbol{\tau}_3$ being the vector pointing from $\boldsymbol{z}_3$ to $\boldsymbol{q}^*$ we have

$$\pm\boldsymbol{\tau}_3 \nabla|_{\tilde{\mathfrak{e}}}(\bar{\chi}_{\tilde{\mathfrak{s}}}^n - w_{\mathfrak{m},1}^n) = 0. \tag{32}$$

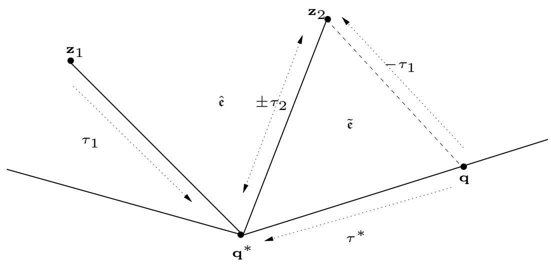

Figure 1: Construction of the linear combination of $\boldsymbol{\tau}_1$

The cut of the plane defined by $\boldsymbol{\tau}^*$ and $\boldsymbol{\tau}_3$ with an interior side $\hat{\mathfrak{s}}$ of another element $\hat{\mathfrak{e}}$ defines $\boldsymbol{\tau}_1$. Let $\boldsymbol{z}_1$ and $\boldsymbol{z}_2$ be the two interior nodes of the interior side $\hat{\mathfrak{s}}$ then we define $\bar{\chi}^n_{\tilde{\mathfrak{s}}}(\boldsymbol{z}_1) = w^n_{\mathfrak{m},1}(\boldsymbol{z}_1)$ and $\bar{\chi}^n_{\tilde{\mathfrak{s}}}(\boldsymbol{z}_2) = w^n_{\mathfrak{m},1}(\boldsymbol{z}_2)$ such that

$$(\bar{\chi}^n_{\tilde{\mathfrak{s}}} - w^n_{\mathfrak{m},1})(\boldsymbol{q}^*) \lesssim h_p \nabla|_{\hat{\mathfrak{e}}}(\bar{\chi}^n_{\tilde{\mathfrak{s}}} - w^n_{\mathfrak{m},1}) \cdot \boldsymbol{\tau_1}$$

as for the two-dimensional case (27). Together with (32) we can draw the same conclusion as in (29, 30, 31)

$$(\bar{\chi}^n_{\tilde{\mathfrak{s}}} - w^n_{\mathfrak{m},1})(\boldsymbol{q}^*) \lesssim h_p \left(\nabla|_{\hat{\mathfrak{e}}}(\bar{\chi}^n_{\tilde{\mathfrak{s}}} - w^n_{\mathfrak{m},1}) - \nabla|_{\tilde{\mathfrak{e}}}(\bar{\chi}^n_{\tilde{\mathfrak{s}}} - w^n_{\mathfrak{m},1})\right) \cdot \boldsymbol{\tau_1}. \tag{33}$$

Let $\mathfrak{e}_0 = \hat{\mathfrak{e}}$, $\mathfrak{e}_m = \tilde{\mathfrak{e}}$ and $\mathfrak{e}_i$ $i = 1, \ldots, m-1$ the elements between. Common sides are denoted by $\mathfrak{s}_i := \mathfrak{e}_{i-1} \cap \mathfrak{e}_i$ and the interelement jumps of gradients by $[\nabla v_{\mathfrak{m}}]^I_{\mathfrak{s}_i} := (\nabla|_{\mathfrak{e}_i} v_{\mathfrak{m}} - \nabla|_{\mathfrak{e}_{i-1}} v_{\mathfrak{m}})$. Thus, for each side $\tilde{\mathfrak{s}}$ the right hand side of (31, 33) can be bounded by the jumps

$$\begin{aligned} h_p| \,\nabla|_{\hat{\mathfrak{e}}}(\bar{\chi}^n_{\tilde{\mathfrak{s}}} - w^n_{\mathfrak{m},1}) - \nabla|_{\tilde{\mathfrak{e}}}(\bar{\chi}^n_{\tilde{\mathfrak{s}}} - w^n_{\mathfrak{m},1})\,| &\lesssim \sum_{i=1}^{m} h_p [\nabla(\bar{\chi}^n_{\tilde{\mathfrak{s}}} - w^n_{\mathfrak{m},1})]^I_{\mathfrak{s}_i} \\ &\lesssim h_p^{\frac{-d+2}{2}} \left(h_p^{\frac{1}{2}} \|[\nabla(\bar{\chi}^n_{\tilde{\mathfrak{s}}} - w^n_{\mathfrak{m},1})]^I\|_{\cup_{\tilde{q}\in\tilde{\mathfrak{s}}}\omega_{\tilde{q}}}\right) \end{aligned}$$

and thus

$$\int_{b_p} \left(\bar{\chi}^n_{\tilde{p}} - w^n_{\mathfrak{m},1}\right) \phi_p \lesssim \sum_{\tilde{\mathfrak{s}}\cap b_p \neq \emptyset} h_p^{\frac{d}{2}} \left(h_p^{\frac{1}{2}} \|[\boldsymbol{\nabla}(\bar{\chi}^n_{\tilde{\mathfrak{s}}} - w^n_{\mathfrak{m},1})]^I\|_{\cup_{\tilde{q}\in\tilde{\mathfrak{s}}}\omega_{\tilde{q}}}\right). \tag{34}$$

Due to the definition of s^n_p

$$\begin{aligned} s^n_p &= \frac{\left\langle \lambda^n_{\mathfrak{m},1}, \phi_p \right\rangle_{-1,1}}{\int_{\gamma_{p,C}} \phi_p} \\ &= \frac{\int_{\tilde{\gamma}_{p,I}} J^I_1(\boldsymbol{u}^n_{\mathfrak{m}})\phi_p + \int_{\tilde{\omega}_p} f^n_1 \phi_p + \int_{\tilde{\gamma}_{p,N}} J^N_1(\boldsymbol{u}^n_{\mathfrak{m}})\phi_p - \int_{\tilde{\gamma}_{p,C}} \hat{\sigma}_1(\boldsymbol{u}^n_{\mathfrak{m}})\phi_p}{\int_{\tilde{\gamma}_{p,C}} \phi_p} \end{aligned}$$

and the fact that η_6 and η_7 have no contributions from the area of full-contact nodes we get a bound

$$s_p^n \lesssim \left(\sum_{k=1}^{5}(\eta_{k,p}^n)\right) h_p^{-\frac{d}{2}} \tag{35}$$

by estimator contributions for which we already derived an upper bound in Sections 5.2 and 5.3. We note that in the case that $\boldsymbol{p}$ would be a full-contact node defined as in [18] $h_p^{\frac{1}{2}} \|\hat{\sigma}_1(\boldsymbol{u}_{\mathfrak{m},1}^n)\|_{\tilde{\gamma}_{p,C}}$ would occur in the upper bound of s_p^n but is not related to the Galerkin functional and other estimator contributions, respectively, see Remark 2. Combining (34) with (35) we arrive at

$$s_p^n \int_{b_p} \left(\chi_{\bar{p}}^n - w_{\mathfrak{m},1}^n\right) \phi_p \lesssim \left(\sum_{k=1}^{5}(\eta_{k,p}^n)^2\right) + \left(\sum_{\tilde{\mathfrak{s}}\cap b_p\neq\emptyset} h_p \|[\boldsymbol{\nabla}(\bar{\chi}_{\tilde{\mathfrak{s}}}^n - w_{\mathfrak{m},1}^n)]^I\|^2_{\cup_{\tilde{q}\in\tilde{\mathfrak{s}}}\omega_{\tilde{q}}}\right). \tag{36}$$

Together with (23, 26) we get

$$\begin{aligned}\left(\left(\eta_{6,p}^n\right)^2 + \left(\eta_{7,p}^n\right)^2\right)^{\frac{1}{2}} &\lesssim \mathrm{ErrMeasL}(\boldsymbol{u}_{\mathfrak{m}}^n, \dot{\boldsymbol{u}}_{\mathfrak{m}}^\tau, \tilde{\boldsymbol{\lambda}}_{\mathfrak{m}}^n) + \mathrm{osc}_p(\boldsymbol{f}^n) + \mathrm{osc}_p(\boldsymbol{\pi}^n) \\ &\quad + \sum_{\tilde{\mathfrak{s}}\cap b_p\neq\emptyset} h_p^{\frac{1}{2}} \|[\boldsymbol{\nabla}(\bar{\chi}_{\tilde{\mathfrak{s}}}^n - w_{\mathfrak{m},1}^n)]^I\|_{\cup_{\tilde{q}\in\tilde{\mathfrak{s}}}\omega_{\tilde{q}}}.\end{aligned} \tag{37}$$

We conclude that Theorem 3 follows from (23, 26, 37).

5.5 Global lower bound

Finally, we aim to bound the estimator globally by the error measure (3.1). From the local estimates (22), (25) and (36) we get directly

$$\begin{aligned}\sum_{k=1}^{7}(\eta_k^n)^2 &\lesssim \|\boldsymbol{\mathcal{G}}_{\mathfrak{m}}^n\|^2_{-1,\Omega} + \sum_p \left(\mathrm{osc}_p^2(\boldsymbol{f}^n) + \mathrm{osc}_p^2(\boldsymbol{\pi}^n)\right) \\ &\quad + \sum_{p\in\mathfrak{N}_{\mathfrak{m}}^{sC}} \sum_{\tilde{\mathfrak{s}}\cap b_p\neq\emptyset} \left(h_p \|[\boldsymbol{\nabla}(\bar{\chi}_{\tilde{\mathfrak{s}}}^n - w_{\mathfrak{m},1}^n)]^I\|^2_{\cup_{\tilde{q}\in\tilde{\mathfrak{s}}}\omega_{\tilde{q}}}\right)\end{aligned}$$

where we used that the local lower bounds imply a global bound (see e.g. [18, Remark 3.8]) . Integrating in time and exploiting (21) we get

$$\begin{aligned}&(\eta_\tau^n)^2 + \sum_{k=1}^{7} \tau^n (\eta_k^n)^2 \\ &\lesssim \|\boldsymbol{\mathcal{G}}_\tau^n\|^2_{L^2([t^{n-1},t^n],H^{-1})} + \|\boldsymbol{\mathcal{G}}_{\mathfrak{m}}^n\|^2_{L^2([t^{n-1},t^n],H^{-1})} \\ &+ \tau^n \sum_p \left(\mathrm{osc}_p^2(\boldsymbol{f}^n) + \mathrm{osc}_p^2(\boldsymbol{\pi}^n)\right) + \tau^n \sum_{p\in\mathfrak{N}_{\mathfrak{m}}^{sC}} \sum_{\tilde{\mathfrak{s}}\cap b_p\neq\emptyset} \left(h_p \|[\boldsymbol{\nabla}(\bar{\chi}_{\tilde{\mathfrak{s}}}^n - w_{\mathfrak{m},1}^n)]^I\|^2_{\cup_{\tilde{q}\in\tilde{\mathfrak{s}}}\omega_{\tilde{q}}}\right).\end{aligned} \tag{38}$$

As the dual norm of the Galerkin functional is bounded by the error measure (7), we make use of the following result

Lemma 2. *There exists a constant β such that the inequality*

$$\beta \left\{ \|\boldsymbol{\mathcal{G}}_\tau^n\|^2_{L^2([t^{n-1},t^n],H^{-1})} + \|\boldsymbol{\mathcal{G}}_{\mathfrak{m}}^n\|^2_{L^2([t^{n-1},t^n],H^{-1})} \right\}^{\frac{1}{2}} \leq \|\boldsymbol{\mathcal{G}}_\tau^n + \boldsymbol{\mathcal{G}}_{\mathfrak{m}}^n\|_{L^2([t^{n-1},t^n],H^{-1})}$$

holds.

which follows from [25, Lemma 6.3] (or [25, Lemma 3.53], respectively). Combining (38),(7),(6) and Lemma 2 leads to the result of Theorem 2

$$\eta^n \lesssim \mathrm{ErrMeasG}(\boldsymbol{u}_{\mathfrak{m}}^\tau, \dot{\boldsymbol{u}}_{\mathfrak{m}}^\tau, \tilde{\boldsymbol{\lambda}}_{\mathfrak{m}}^\tau, [t^{n-1}, t^n]) + \|\tilde{\boldsymbol{f}} - \tilde{\boldsymbol{f}}^\tau\|_{L^2([t^{n-1},t^n],H^{-1})}$$
$$+ \sqrt{\tau^n} \left(\sum_{p \in \mathfrak{N}_{\mathfrak{m}}} \mathrm{osc}_p^2(\boldsymbol{f}^n) + \sum_{p \in \mathfrak{N}_{\mathfrak{m}}^N} \mathrm{osc}_p^2(\boldsymbol{\pi}^n) + \sum_{p \in \mathfrak{N}_{\mathfrak{m}}^{sC}} \sum_{\tilde{\mathfrak{s}} \cap b_p \neq \emptyset} \left(h_p \|[\boldsymbol{\nabla}(\bar{\chi}_{\tilde{\mathfrak{s}}}^n - w_{\mathfrak{m},1}^n)]^I\|^2_{\cup_{\tilde{q} \in \tilde{\mathfrak{s}}} \omega_{\tilde{q}}} \right) \right)^{\frac{1}{2}}.$$

6 Numerical results

The implementation has been carried out in MATLAB. As basis for the implementation of the adaptive mesh generation we have used [10, Chapter 5] as well as [2]. As solver for the variational inequalities we implemented a primal-dual-active set method similar to [3, Chapter 5.3.1].

We use newest vertex bisection as refinement strategy and the maximum strategy as marking strategy. We denote by $\mathfrak{M}_{k+1}$ the refined or coarsened mesh succeeding $\mathfrak{M}_k$. In each time step n the starting mesh $\mathfrak{M}_0^n$ is the final mesh $\mathfrak{M}^{n-1}$ of time step $n-1$.

First, we conduct some coarsening steps if the interpolation error obtained by replacing $\boldsymbol{u}_{\mathfrak{m}_k}^{n-1}$ with $I(\boldsymbol{u}_{\mathfrak{m}_{k+1}}^{n-1})$ in the residual is a small percentage of the estimator of the foregoing time step. Next, we start the refinement process in the new time step n based on the spatial estimator $\eta_{\mathfrak{m}}^n$. The refinement process stops if a given maximal number of elements has been passed over in the foregoing iteration step or if the estimator $\eta_{\mathfrak{m}}^n$ is very small. Finally, we compute the temporal estimator. If the temporal estimator is larger or significantly smaller than the spatial estimator we reduce or increase the time step size, restore the mesh from the foregoing time step and start the adaptive mesh refinement in time step n, newly. Otherwise, we accept the mesh and the time step size and continue with time step $n+1$.

6.1 Contact with a wedge

We simulate the deformation of a linear viscoelastic unit square which is moved via time-dependent Dirichlet boundary conditions $u_{D,1} = (0.1 - t)$ at $x = 0$ towards the obstacle $g(y) = -0.2 + 0.5 \cdot |y - 0.5|$ which describes a wedge with a semi-angle $\alpha \approx 63$. We consider two examples with different sets of material parameters. In the first example we choose the Young's modulus $E = 2 \cdot 10^5$, the Poisson ratio $\nu = 0.25$, the shear viscosity $\eta = 5 \cdot 10^{-2}$ and the bulk viscosity $\zeta = 5 \cdot 10^{-2}$. In the second example we choose $E = 500$, $\nu = 0.3$ and $\eta = 30$, $\zeta = 30$. The maximal number of elements which has to be passed before the refinement process stops is set to 5000 elements. In both cases the time step is $\tau = 0.03$ and is not changed.

For the first example we show the deformed configuration and the adaptively refined meshes in the area $[0.2, 1.0] \times [0.1, 0.9]$ at times $t = 0.03$, $t = 0.12$

and $t = 0.27$ in Figure 2. At time $t = 0.03$ and $t = 0.12$ it is obvious that the adaptive refinement is strong where the tip of the wedge indents and at the free boundary whereas not the whole contact zone is highly refined. We note that the body detaches at time $t = 0.3$. Thus, at time $t = 0.27$ the area of contact coincides with the area where the tip of the wedge indents and thus this effect cannot be seen. In Figure 3 we plot the estimator against the number of nodes with logarithmic scales to show the experimental order of convergence at times $t = 0.03$, $t = 0.12$ and $t = 0.27$. At the first time step we compare also with uniform refinement. At the following time steps there are less adaptive refinement steps as we do not start again from the coarsest mesh. The experimental order of convergence is ≈ 0.5 in the case of adaptive refinement and in contrast ≈ 0.3 in the case of uniform refinement.
For the first example we list in Table 1 and Table 2 the estimator contribution referring to the complementarity residual $\sqrt{\tau^n\left(\left(\eta^n_{\mathfrak{m}_k,6}\right)^2+\left(\eta^n_{\mathfrak{m}_k,7}\right)^2\right)}$ and the sum of the spatial estimator contributions $\sqrt{\tau^n}\eta^n_{\mathfrak{m}_k}$ in time steps $n = 1$ and $n = 6$. As stated in Remark 3 the complementarity residual is much smaller than the spatial estimator. The difference is about 10^4.

Table 1: Comparison of spatial estimator and complementarity residual in time step $n = 1$

k	$\sqrt{\tau^1\left(\left(\eta^1_{\mathfrak{m}_k,6}\right)^2+\left(\eta^1_{\mathfrak{m}_k,7}\right)^2\right)}$	$\sqrt{\tau^1}\eta^1_{\mathfrak{m}_k}$
$k=1$	5.1297	$1.9124 \cdot 10^4$
$k=2$	1.0733	$0.9896 \cdot 10^4$
$k=3$	0.4801	$0.7496 \cdot 10^4$
$k=4$	0.4588	$0.6334 \cdot 10^4$
$k=5$	0.3919	$0.4896 \cdot 10^4$
$k=6$	0.3782	$0.3649 \cdot 10^4$
$k=7$	0.1355	$0.3113 \cdot 10^4$
$k=8$	0.0509	$0.2226 \cdot 10^4$
$k=9$	0.0423	$0.1758 \cdot 10^4$
$k=10$	0.0429	$0.1270 \cdot 10^4$
$k=11$	0.0177	$0.0987 \cdot 10^4$

Table 2: Comparison of spatial estimator and complementarity residual in time step $n = 6$

k	$\sqrt{\tau^6\left(\left(\eta^6_{\mathfrak{m}_k,6}\right)^2+\left(\eta^6_{\mathfrak{m}_k,7}\right)^2\right)}$	$\sqrt{\tau^6}\eta^6_{\mathfrak{m}_k}$
$k=1$	0.0109	546.4735
$k=2$	0.0027	490.6460
$k=3$	0.0016	295.4914

Due to the different material parameters in the second example the deformation

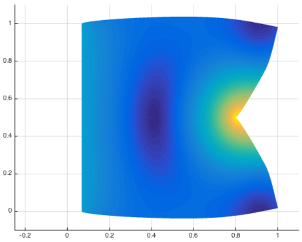

(a) *deformation* $t = 0.03$

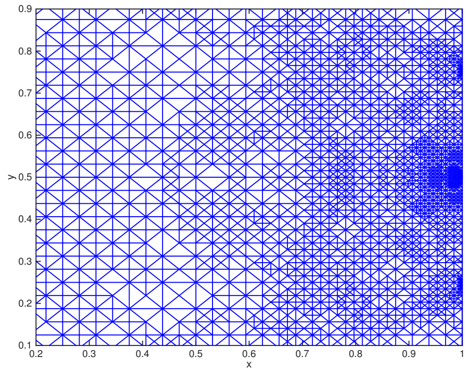

(b) *mesh* $t = 0.03$

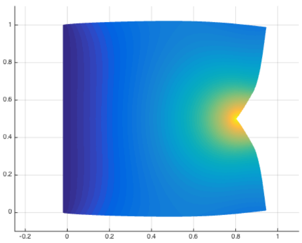

(c) *deformation* $t = 0.12$

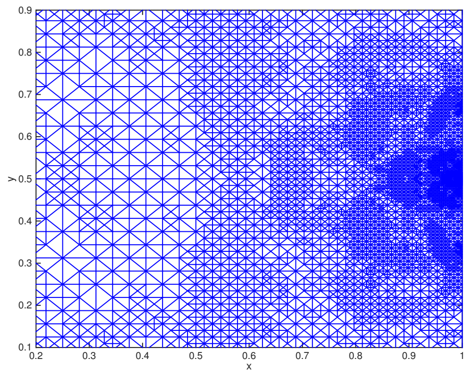

(d) *mesh* $t = 0.12$

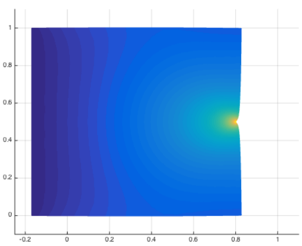

(e) *deformation* $t = 0.27$

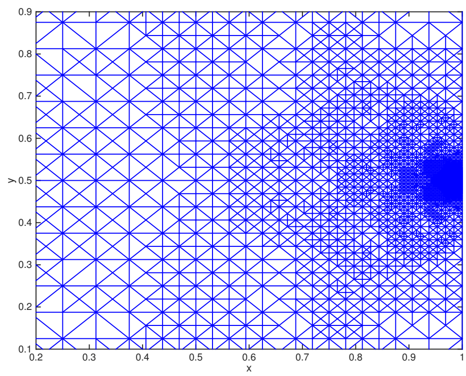

(f) *mesh* $t = 0.27$

Figure 2: Indentation by a wedge (first example): Deformation and adaptively refined mesh

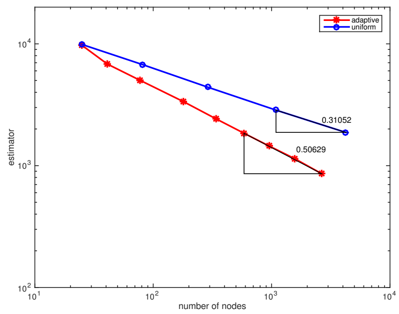

(a) $t = 0.03$

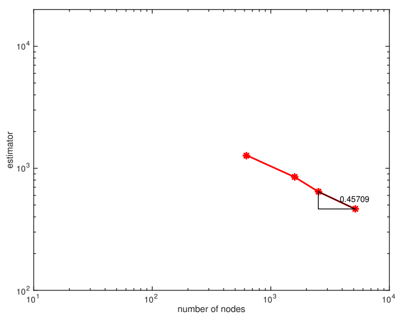

(b) $t = 0.12$

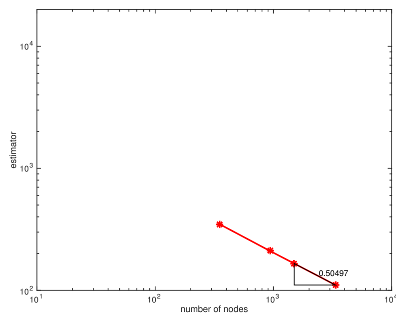

(c) $t = 0.27$

Figure 3: Indentation by a wedge (first example): Convergence of estimator

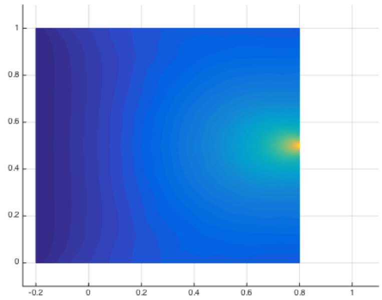

(a) $E = 2 \cdot 10^5$, $\nu = 0.25$, $\eta = \zeta = 5 \cdot 10^{-2}$

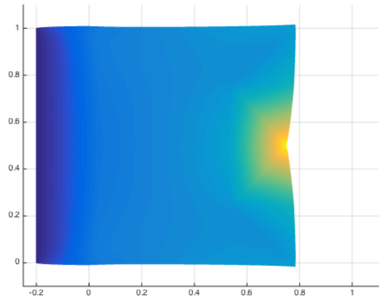

(b) $E = 500$, $\nu = 0.3$, $\eta = \zeta = 30$

Figure 4: Comparison of deformation for different material parameters at detachment time $t = 0.03$

which depends on the elastic as well as viscous stress develops differently in time. In the second example there is still a significant deformation at detachment time $t = 0.3$, see Figure 4. In Figure 5 we show for the second example the adaptively refined meshes and we plot the estimator against the number of nodes at times $t = 0.03$, $t = 0.15$ and $t = 0.27$. In order to visualize the experimental order of convergence we use logarithmic scales. At the first time step we compare also with uniform refinement. The experimental order of convergence varies between ≈ 0.45 and ≈ 0.49 for adaptive refinement and is ≈ 0.33 for uniform refinement.

6.2 Contact with a parable

In the third example we simulate the deformation of a linear viscoelastic unit square which may come into contact with a parable depending on a time-dependent force term $\boldsymbol{f}$. The obstacle is described by $g(y) = (y - 0.5)^2$ at the right hand side $x = 1$ and the Dirichlet values by $u_{D,1} = 0$ at the left hand side $x = 0$. The right hand side is given by

$$\begin{aligned} f_1 = &(\sin(10t\pi))(-2(\lambda + 2\mu)(y - y^2) - 2\mu(x - x^2)) \\ &+ 10\pi(\cos(10t\pi))(-2(\lambda_V + 2\eta)(y - y^2) - 2\eta(x - x^2)) \end{aligned}$$

and

$$\begin{aligned} f_2 = &(\sin(10t\pi))(\mu(1 - 2y)(1 - 2x) + \lambda(1 - 2x)(1 - 2y)) \\ &+ 10\pi(\cos(10t\pi))(\eta(1 - 2y)(1 - 2x) + \lambda_V(1 - 2x)(1 - 2y)). \end{aligned}$$

In the case no contact occurs the right hand side corresponds to the solution $u_1 = \sin(10t\pi)x(1 - x)y(1 - y)$, $u_2 = 0$. The material parameters are chosen as in the first example. In Figure 6 we visualize the solution $u_{\mathfrak{m},1}$ at different times. We start with a time step size $\tau = 0.05$ but due to the time-dependent right hand side the time step size will be adapted and thus varies between 0.05 and $7.8125 \cdot 10^{-4}$. The maximal number of elements which has to be passed before the refinement process stops in each time step is set to 5000 elements.

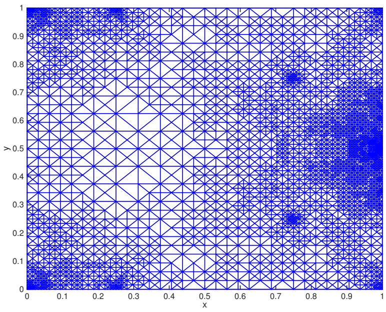

(a) *mesh* $t = 0.03$

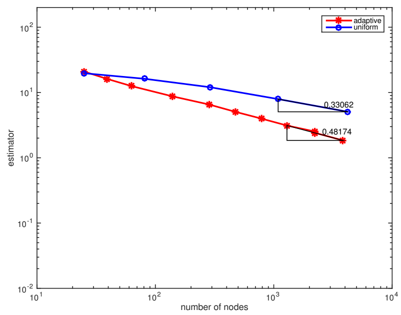

(b) *experimental order of convergence* $t = 0.03$

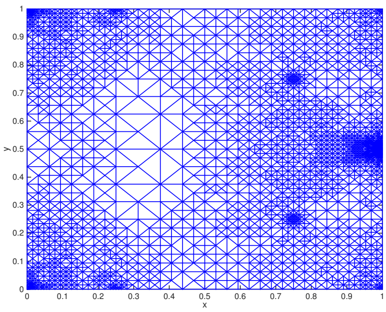

(c) *mesh* $t = 0.15$

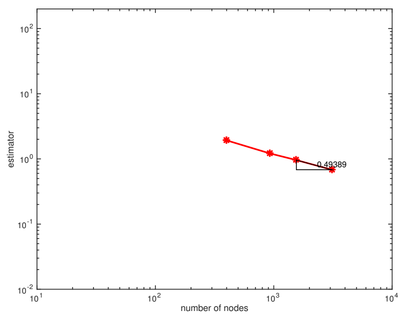

(d) *experimental order of convergence* $t = 0.15$

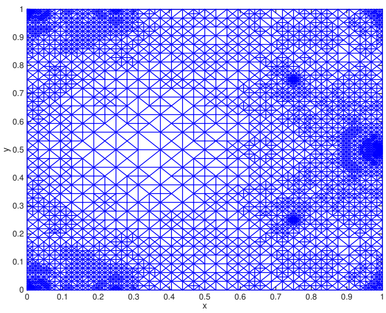

(e) *mesh* $t = 0.27$

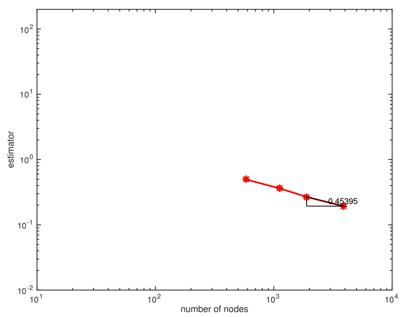

(f) *experimental order of convergence* $t = 0.27$

Figure 5: Indentation by a wedge (second example): Adaptively refined mesh and experimental order of convergence

In this case $\left(\sum_n \tau^n \left(\eta_{\mathfrak{m}}^n\right)^2\right)^{\frac{1}{2}} = 1.8123 \cdot 10^3$. Reducing the maximal number of elements which has to be passed before the refinement process stops to 2000 or 500 increases the spatial estimator to $\left(\sum_n \tau^n \left(\eta_{\mathfrak{m}}^n\right)^2\right)^{\frac{1}{2}} = 3.2498 \cdot 10^3$ or $\left(\sum_n \tau^n \left(\eta_{\mathfrak{m}}^n\right)^2\right)^{\frac{1}{2}} = 6.1488 \cdot 10^3$, respectively.

References

[1] Arendt, W., Batty, C., Hieber, M., Neubrander, F.: Vector-valued Laplace transforms and Cauchy problems, Monographs in Mathematics, Vol. 96, Birkhäuser/Springer Basel AG, Basel (2011).

[2] Bartels, S., Schreier, P.: Local coarsening of simplicial finite element meshes generated by bisections. BIT. Numerical Mathematics, 52 (3), pp. 559–569 (2012).

[3] Bartels, S.: Numerical Methods for Nonlinear Partial Differential Equations. Springer Ser. Comput. Math. 47, Springer, Cham (2015).

[4] Barbu, V..: Nonlinear differential equations of monotone types in Banach spaces. Springer Monographs in Mathematics, New York (2010).

[5] Dill, E.H.: Continuum Mechanics: Elasticity, Plasticity, and Viscoelasticity CRC Press (2006)

[6] Eck, C.: Existenz und Regularität der Lösungen für Kontaktprobleme mit Reibung. PhD thesis, Mathematisches Institut der Universität Stuttgart (1996)

[7] Fernández, J., Hild, P.: A priori and a posteriori error analysis in the study of viscoelastic problems. Journal of Computational and Applied Mathematics, 225 (2), pp. 569–580 (2009).

[8] Fernández, J., Martinez, R.: A normal compliance contact problem in viscoelasticity: An a posteriori error analysis and computational experiments. Journal of Computational and Applied Mathematics, 235, pp. 3599-3614 (2011).

[9] Fierro, F., Veeser, A.: A posteriori error estimators for regularized total variation of characteristic functions. SIAM J. Numer. Anal. 41, 2032–2055 (2003)

[10] Funken, S., Praetorius, D., Wissgott, P.: Efficient implementation of adaptive P1-FEM Matlab . Comput. Methods Appl. Math. 11, 460-490 (2011)

[11] Gudi, T., Porwal, K.: A posteriori error control of discontinuous Galerkin methods for elliptic obstacle problems. Math. Comp. 83, 579-602 (2014)

[12] Gudi, T., Porwal, K.: A posteriori error estimates of discontinuous Galerkin methods for the Signorini problem. J. Comput. Appl. Math. 292, 257-278 (2016)

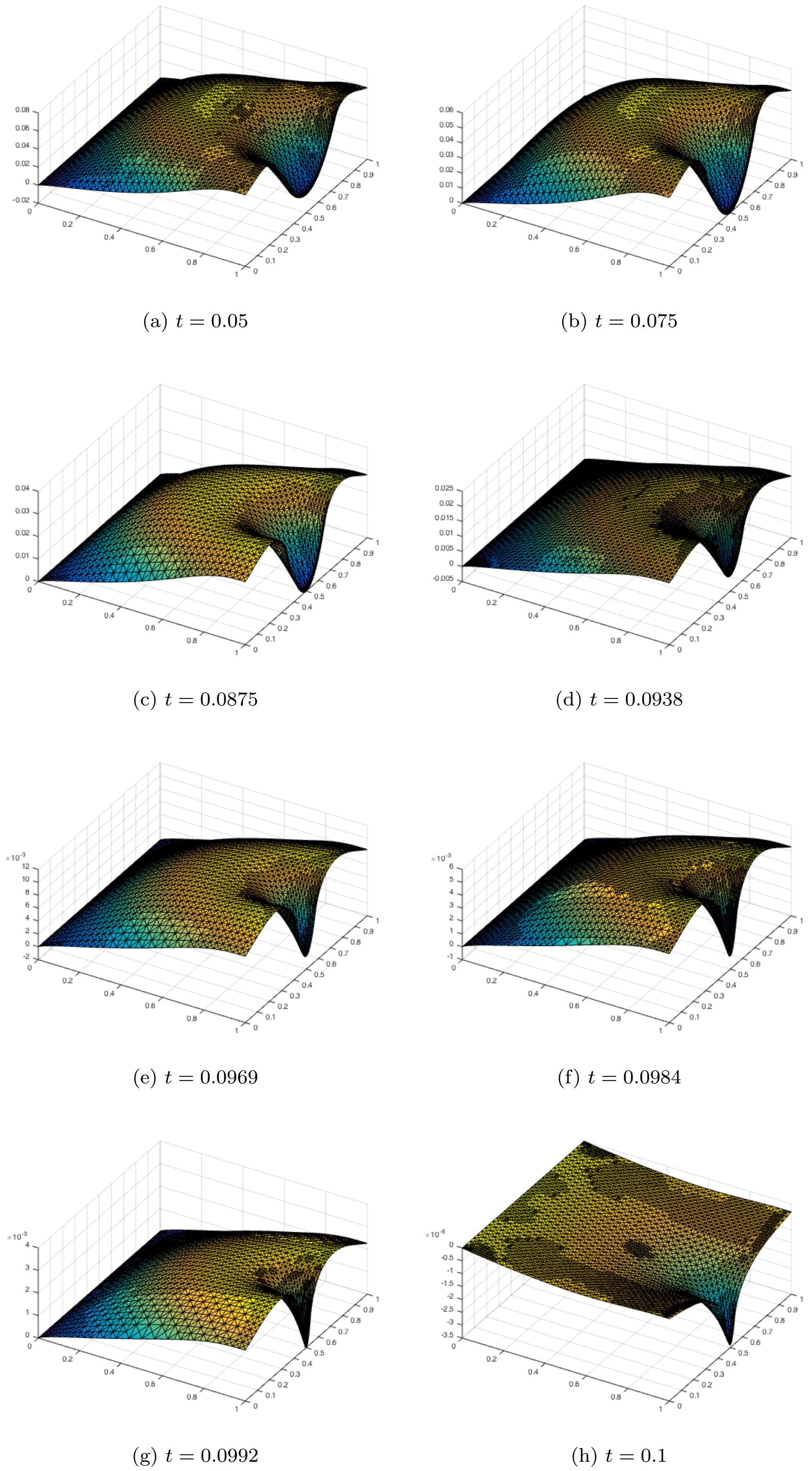

(a) $t = 0.05$ (b) $t = 0.075$

(c) $t = 0.0875$ (d) $t = 0.0938$

(e) $t = 0.0969$ (f) $t = 0.0984$

(g) $t = 0.0992$ (h) $t = 0.1$

Figure 6: First coordinate of solution $u_{\mathfrak{m},1}$ on adaptively refined mesh

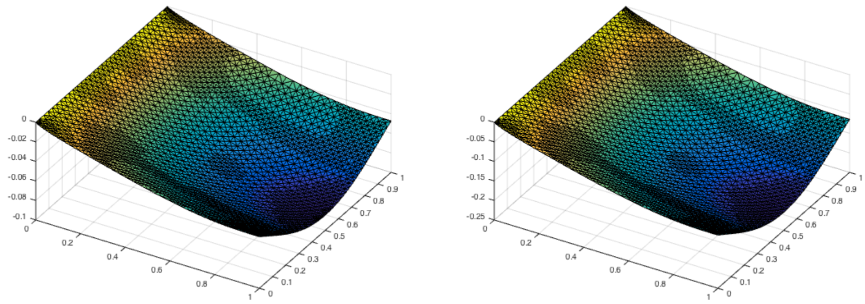

(i) $t = 0.1125$ (j) $t = 0.1625$

Figure 6: First coordinate of solution $u_{\mathrm{m},1}$ on adaptively refined mesh

[13] Han, W., Sofonea, M.: Quasistatic contact problems in viscoelasticity and viscoplasticity. In AMS/IP Studies in Advanced Mathematics, Volume 30, American Mathematical Society: Providence, RI (2002).

[14] Hild, P., Nicaise, S.: Residual a posteriori error estimators for contact problems in elasticity. M2AN Math. Model. Numer. Anal. 41, 897–923 (2007)

[15] Kikuchi, N., Oden, J.: Contact problems in elasticity: a study of variational inequalities and finite element methods. SIAM, Philadelphia, PA (1988)

[16] Krause, R., Veeser, A., Walloth, M.: An efficient and reliable residual-type a posteriori error estimator for the Signorini problem. Numer. Math. 130, 151-197 (2015)

[17] Lions, J., Stampacchia, G.: Variational inequalities. Communications on Pure and Applied Mathematics, 20 (), 493–519, 1976.

[18] Moon, K., Nochetto, R., von Petersdorff, T., Zhang, C.: A posteriori error analysis for parabolic variational inequalities. M2AN Math. Model. Numer. Anal. 41, 485–511 (2007)

[19] Nochetto, R., Siebert, K. and Veeser, A.: Pointwise a posteriori error control for elliptic obstacle problems. Numer. Math. 95, 163–195 (2003)

[20] Nochetto, R., Siebert, K. and Veeser, A.: Fully localized a posteriori error estimators and barrier sets for contact problems. SIAM J. Numer. Anal. 42, 2118–2135 (2005)

[21] Siebert, K., Veeser, A.: A unilaterally constrained quadratic minimization with adaptive finite elements. SIAM J. Optim. 18, 260–289 (2007)

[22] Veeser, A.: Efficient and reliable a posteriori error estimators for elliptic obstacle problems. SIAM J. Numer. Anal. 39, 146–167 (2001)

[23] Verfürth, R.: A review of a posteriori error estimation techniques for elasticity problems. Comp. Meth. Appl. Mech. Engrg. 176, 419-440 (1999)

[24] Verfuerth, R.: A posteriori error estimates for finite element discretizations of the heat equation. Calcolo. A Quarterly on Numerical Analysis and Theory of Computation, 40 (3), pp. 195–212 (2003).

[25] Verfürth, R.: A Posteriori Error Estimation Techniques for Finite Element Methods. Oxford University Press (2013)

[26] Walloth, M.: Adaptive numerical simulation of contact problems: Resolving local effects at the contact boundary in space and time. PhD thesis, Rheinische Friedrich-Wilhelms-Universität Bonn (2012)

[27] Walloth, M.: A reliable, efficient and localized error estimator for a discontinuous Galerkin method for the Signorini problem. Preprint 2713, Fachbereich Mathematik, TU Darmstadt (2016)

[28] Wloka, J.: Partielle Differentialgleichungen, Teubner, Stuttgart (1982)